DEVELOPMENT OF A COMPTON-SCATTERING-BASED BEAM-INTENSITY MONITOR AT THE HIGS FACILITY

by

Brendan Timothy Crowley

Department of Physics
Duke University

Date: _____

Approved:

_____
Dr. Henry Weller, Supervisor

_____
Dr. Vladimir Litvinenko

_____
Dr. M. Ronen Plesser

A thesis submitted in partial fulfillment of the
requirements for the degree of Master of Science
in the Department of Physics
in the Graduate School of
Duke University

2001

Abstract

The collaboration of the Duke Free-Electron Laser Laboratory and Triangle Universities Nuclear Laboratory is developing a program to study many exciting aspects of nuclear physics using a high-intensity 100% polarized γ-ray beam which is nearly monochromatic and can be tuned over a certain energy range. Some of the experiments planned for this program will require a knowledge of the absolute flux of these γ rays to an accuracy of 1-2%. Due to the unique nature of this beam, the measurement of the flux becomes a non-trivial problem. Specifically, the high intensity of the beam makes it very useful for studying nuclear processes, but makes it challenging to directly measure the flux by placing a detector directly in the beam due to the limited maximum counting rate of standard γ-ray detectors. The flux is currently as high $10^7\gamma/sec$ and is expected to increase in the near future with upgrades planned for the facility.

This thesis describes the development of a technique to make an indirect measure of the γ-ray flux by placing a thin scattering foil in the beam and then detecting the Compton-scattered γ rays at a particular scattering angle using a collimated 10" x 10" NaI detector. This experiment was performed at incident γ-ray energies of 10 and 15 MeV with various scattering targets and scattering angles. Simultaneously, another NaI detector was placed directly in the beam (after several inches of lead attenuation) to make a direct measurement. After data were taken and analyzed it was possible to extract correction factors to the raw count rate in the off-axis NaI detector which correlate it with the flux deduced by the direct flux method, which is still reliable at these fluxes. The estimated uncertainty in the fluxes deduced using this technique is approximately 5%. A discussion of ways to improve on this technique in the future for its implementation as a measure of the flux will be given.

Acknowledgements

I'd like to start by thanking my advisor, Henry Weller. He was always supportive and helpful in all of my experiences at Duke. I'd also like to thank Ronen Plesser for reading my thesis and listening to my talk, and Vladimir Litvinenko for correcting all of my mistakes and teaching me everything I ever wanted to know about the FEL but was afraid to ask.

I'd also like to thank all of the other members of the Capture Group. First, thank you to all of the post docs and other professors including Caroline, Ned, Anton, Dick Prior, Mark Spraker, Kara Keeter, and Ron Tilley. I'd also like to thank all of the grad students in the group: Wulf, Schreiber, Shane, Steve-O, and Konstantin and Amanda. I'd especially like to give an extra big thanks to the last two for their enormous help in nearly every aspect of this thesis. And thanks to Schreiber for helping me so much at the FEL. Shane, your thesis brought me to tears.

I can't forget to thank all of my friends from the Great White North (Brad, Ru, and Norm) who were a tremendous help with my experiment. I hope you forgive me for all the jokes I made about the fact that you're Canadien, eh.

There are many others that I would like to thank. Paul H., for always believing in me. Patrick, ever since our days of playing hockey together you always taught

me that sometimes the best decision is to let some goals just pass on by. Matt Hooper from the Oceanographic Institute, you're a great friend. Maurice, thanks for providing me with all of those γ rays.

And lastly I'd like to thank my parents and my four older brothers, except for Devon. And I'd like to thank Liz for sticking with me for the past five years, and hopefully you'll stick with me for a few more.

Contents

List of Tables

List of Figures

Chapter 1

Introduction

Many different experiments in photonuclear physics using a high-intensity gamma-ray beam will be performed at the Duke Free-Electron Laser Laboratory in the near future - all of which will require a precise knowledge of the flux of this beam. The unique nature of this γ-ray beam makes conventional "in-beam" measurements of the flux unreliable, therefore the need for an equally unique method for measuring the flux is of great importance. The results of a Compton scattering experiment which was developed as a flux monitor for a high-intensity γ-ray beam at the Duke Free-Electron Laser Laboratory (DFELL) are presented in this thesis. Throughout this thesis, the term "flux" will refer to the number of γ rays in the beam per unit time.

1.1 Overview

The HIGS (High-Intensity Gamma-ray Source) program is a collaborative program between the Duke Free-Electron Laser Laboratory and Triangle Universities Nuclear Laboratory (TUNL). This facility provides a cutting-edge tool for investigating many different and exciting aspects of nuclear physics. There are only a handful of institutions in the world which use electromagnetic probes to study the nucleus and the HIGS program has the potential to provide some of the most complete data sets in the field of photonuclear physics. DFELL is currently capable of providing a γ-ray beam with an energy range of 2-60 MeV, and, with a planned upgrade, this range will be extended up to 225 MeV.

1.1.1 Possible Experiments

An understanding of nuclear and particle physics begins with an understanding of the strong force through Quantum Chromodynamics (QCD). However, although a direct solution to the QCD lagrangian has not been achieved, recent effective field theories (EFT) are a promising step to study low energy nuclear physics in the context of QCD. Effective field theories are theories which do not account for all the degrees of freedom in a system, rather they include these degrees of freedom as "effective" interactions while exploiting the symmetries of some theory, which in our case is QCD.

Chiral Perturbation Theory (ChPT) is an effective field theory which bases itself on the existence of chiral symmetry in QCD. Since ChPT is a low energy EFT (below 500 MeV), HIGS can test the consistency of predictions made by ChPT with experimentally observed phenomena at these low energies and, thereby, gain a better understanding of the low energy interactions of pions, nucleons, and photons. One such prediction is the values of the electric and magnetic polarizabilities of nucleons. These fundamental structure constants give direct information as to the internal structure of nucleons. Recent attempts to measure these polarizabilities have been accomplished by Compton scattering γ rays from the nucleons and looking for deviations from the scattering cross section of structureless nucleons [Mac95]. This deviation is an extremely small effect at these energies and requires an incident flux of 10^7 γ/sec/MeV in order to be done in a reasonable amount of time. This experiment will be performed at HIGS in the near future, and, since it is a measurement of a cross section, it will require a very precise knowledge of the incident flux ($\pm 1\%$). Other experiments, which are very important to nuclear astrophysics, planned for HIGS also require the precise measurement of cross sections.

The study of astrophysically relevant cross sections in nuclear astrophysics has

been partly dominated by the measurement of radiative capture reactions. A radiative capture reaction is one in which the incident particle is "captured" by the target nucleus, leaving a residual nucleus and the emission of a γ-ray. In stellar burning, these radiative capture reactions occur at very low energies (<1MeV) which, for a variety of reasons, are difficult to measure in the lab so they are measured at slightly higher energies (<5MeV) and the cross sections are extrapolated down to the energy of interest. Even at these slightly higher energies, capture cross section measurements can be difficult to perform. However, the principle of detailed balance directly relates the capture cross section to its inverse reaction, photodisintegration. At HIGS it is possible to escape the difficulties of capture reactions by studying these inverse reactions, where the incident particle is a γ-ray. One such reaction, which is important to the helium burning phase of a red giant star, is $^{12}C(\alpha, \gamma)^{16}O$. The inverse can be studied with a ^{16}O target and a high flux of 10 MeV γ rays.

Another possible measurement would be a precise measurement of the photodisintegration cross section of the deuteron. The deuteron is one of the most basic systems in nuclear physics and has been extensively studied, mainly through n-p capture experiments using neutron beams and thermal neutron capture on hydrogen. One energy region which is lacking data, however, is where the neutron's center-of-mass energy is a few hundred keV. Knowledge of the cross section at these energies is of extreme importance to Big Bang Nucleosynthesis. It is believed that the production of the first deuterium occured at these neutron energies just after the Big Bang. The relative yields of all the primordial light elements are directly related to the n-p capture cross section at these energies. It seems that photodisintegration of the deuteron is the only feasible way to measure the cross section at these low energies, which correspond to γ-ray energies between 2.5-10 MeV. This is within the operating range for the Duke Free-Electron Laser Lab, and, with a reliable measure

of the flux, an absolute cross section measurement could be performed.

1.2 The Duke Free-Electron Laser Laboratory

A free-electron laser (FEL) is a source of highly monochromatic photons whose energy is tunable over a certain range. The free-electron laser at Duke is a storage ring FEL which is capable of producing intense, monochromatic beams of γ rays which are nearly 100% polarized. A brief description of the fundamental principles of how the free-electron laser at DFELL operates is given below.

1.2.1 The Basics of FEL Operation

All free-electron lasers consist of three major components: a source of relativistic electrons, a magnetic wiggler, and an optical cavity. An electron bunch, either inside a storage ring or from a linear accelerator, is accelerated towards a region of alternating magnetic fields (the wiggler). Upon entering this region, the electrons are accelerated back and forth and, therefore, emit radiation. The photons radiated are then captured in an optical cavity. Consequent electron bunches amplify this radiation which is bouncing back and forth inside the optical cavity. If the electron bunch and the photon bunch are properly synchronized so that they enter the FEL region at the same time, the resulting radiation is coherent (this process will be discussed in more detail later in this section). The wavelength of the FEL photons generated depends on the electron beam energy and the parameters of the wiggler, which will also be discussed later.

In standard operating mode, a free-electron laser provides a high-powered beam of coherent radiation which is highly monochromatic and 100% polarized. Since all of the experimental work done in this thesis was performed at the Duke Free-Electron Laser Laboratory (shown in Figure 1.1), the more detailed discussion of the principles

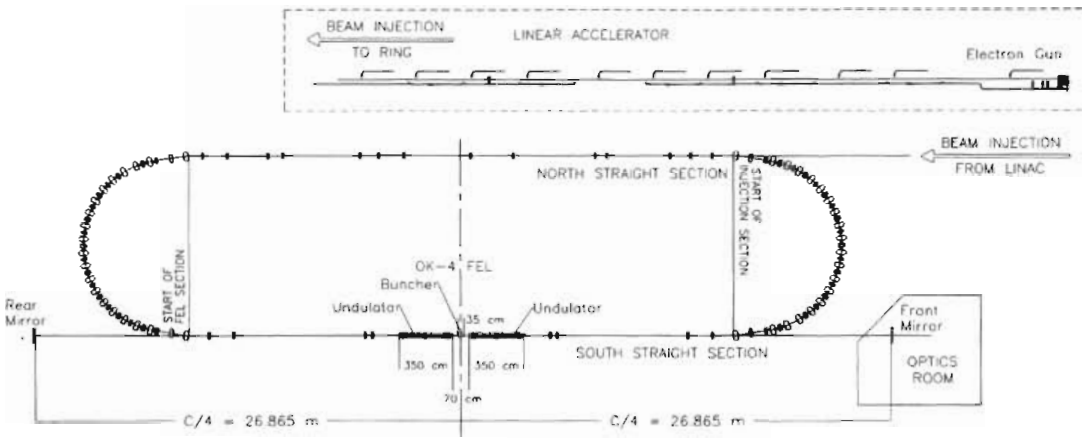

Figure 1.1: Layout of the Duke Free-Electron Laser Laboratory. Figure taken from [Lit95].

of operation will be limited to this particular free-electron laser.

The four major components of the Duke free-electron laser are a linear accelerator, a storage ring, an optical klystron, and an optical cavity. The electron source at DFELL is a linear accelerator which injects the electrons into the storage ring. This linear accelerator is a remnant of the former SLAC Mark III accelerator. It consists of eleven sections, three klystrons, and a photoinjector. It is capable of injecting up to $6x10^8$ electrons/sec at energies up to 270 MeV into the storage ring. Most experiments planned for HIGS will require a higher electron energy, and the electrons can be "ramped" to energies up to 1.1 GeV once inside the storage ring. The "ramping" is not an ideal operating condition because it does not allow continuous injection at all energies. Continuous injection can compensate for the natural decay of the current in the ring by providing more electrons as the others are lost.

The storage ring at DFELL is designed to operate with an electron energy up to 1.1 GeV and to store up to 1.0 Amp of current. It contains 40 dipole magnets for steering the beam and 64 quadrupole magnets which are used for focusing the electron

bunches. The ring also contains an RF cavity which operates at a frequency of 178.547 MHz. This cavity compensates for the loss of electron energy to synchrotron radiation and compresses the electrons into short bunches (1cm). The RF cavity is installed in the middle of the north straight section, the south straight section is dedicated to the optical klystron (OK-4).

The OK-4 optical klystron consists of two wigglers separated by a bunching section. A wiggler has alternating magnetic fields which cause the electrons to emit photons with a wavelength λ_o which is given by the following relation:

$$\lambda_o = \frac{\lambda_w}{2\gamma^2}\left[1 + \frac{1}{2}\left(\frac{\lambda_w e B_\perp}{2\pi m_e c^2}\right)^2\right] = \frac{\lambda_w}{2\gamma^2}\left[1 + \frac{K_w^2}{2}\right], \tag{1.1}$$

where e is the electron charge, γ is the relativistic factor for the electrons, λ_w is the length of one wiggler period, $B_\perp$ is the peak value of the magnetic field, and $m_e c^2$ is the rest energy of the electron [Mar85]. K_w is a dimensionless parameter called the wiggler parameter. In the OK-4 wiggler, K_w can be varied between 0 and 5.42 [Lit93]. The magnetic fields are set-up such that the electrons undergo a transverse oscillation. The next electron bunch arrives at this region at the same time as the previously emitted fel photons so that they copropagate through the undulator region. The electron's motion in the wiggler is in resonance with the optical field when Equation 1.1 is satisfied. The exchange of the energy between the electrons and the optical wave causes an energy modulation of the electrons with a period λ_o. The buncher transfers the energy modulation to density modulation. The bunched electrons then radiate coherently in the second wiggler and amplify the optical (FEL) wave. The plane in which the electrons oscillate determines the polarization of the emitted radiation. Therefore the fel photons are 100% linearly polarized in the horizontal plane when planar wigglers are used.

The present optical cavity consists of two mirrors separated by 53.73 m, which

is half the circumference of the storage ring. This ensures that the photons and electrons enter the undulator at the same time, although fine tuning of the timing is required. The containment of the fel photons in such a long optical cavity is a technical challenge since any misalignment, vibration, or thermal stress on the mirrors can stop the lasing. The mirrors and their mounts are therefore mechanically isolated from the rest of the building, and are mounted to a concrete slab which is resting upon ultra-fine sand.

The type of mirror used for any given experiment defines the available wavelength range of the fel photons. The broad spectral range of the fel photons requires mirrors with different surface coatings in order to maximize reflectivity for the given wavelength. The typical mirrors used in this experiment had a multilayer dielectric coating consisting of SiO_2 and HfO_2 on a fused UV quartz substrate. Each mirror had about 99% reflectivity at 240 nm.

The Duke Free-Electron Laser Lab is going to implement some exciting improvements to their facility in the near future. This includes augmenting the linear accelerator with a booster injector synchrotron which will be able to inject electrons at energies up to 1.2 GeV into the Duke storage ring. There are also plans to replace the OK-4 FEL with the 24 m OK-5 FEL which will generate photons with a desirable polarization - from linear to circular. A schematic of DFELL with these new additions is shown in Figure 1.2.

1.2.2 Compton Backscattering

Most facilities which produce γ-ray beams by Compton backscattering use conventional lasers to scatter low energy photons from ultrarelativistic electrons. The Duke Free-Electron Laser Lab uses intracavity backscattering with the electrons in the ring and the fel-produced photons. HIGS currently has the ability to produce 3-60 MeV γ

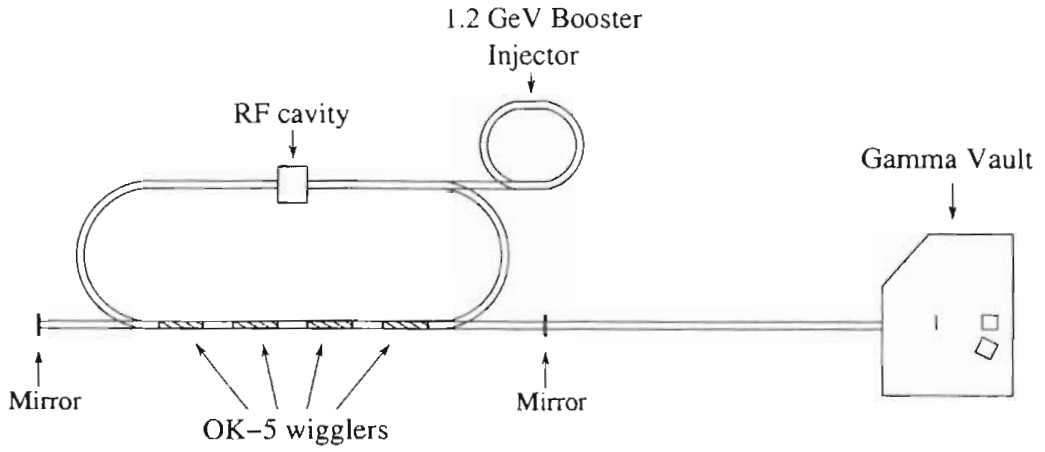

Figure 1.2: Schematic of the Duke Free-Electron Laser Laboratory with the new booster injector and OK-5 included. Figure not drawn to scale.

rays at a flux of 10^6 γ/sec through a collimator. This flux is substantially larger than that produced using conventional lasers as a result of the fact that the scattering at HIGS occurs inside the cavity where the power is higher.

In addition to timing the electron bunches so that they copropagate with the fel photons, it is possible to introduce a second electron bunch that is 180° out of phase with the first. In this operating mode, the second electron bunch reaches the center of the FEL at the same time as the fel photons, travelling in the opposite direction. These photons Compton scatter from the electrons, thereby producing γ rays which are projected into a narrow cone centered on the electron axis. For example, a 3.296 eV photon scattered from a 450 MeV electron produces a 10 MeV γ-ray. The γ rays in the center cone retain the original polarization of the fel photons. So, while the γ-ray beam is not coherent, a high flux of highly monochromatic, 100% polarized γ rays are produced whose energy is tunable within a certain range by varying the energy of the FEL photons (from 2 eV to 6 eV) and the electron beam energy (from 240 MeV to 1.1 GeV).

1.2.3 Energy Resolution

The simplest picture of Compton scattering is when a photon is incident on an electron at rest, and the photon scatters at some angle, θ, while the electron recoils at a different angle, φ. Using conservation of energy and momentum, the energy of the scattered photon as a function of its scattering angle is given by:

$$E' = \frac{E}{1 + \frac{E}{m_e c^2}(1 - cos\theta)}, \tag{1.2}$$

where E' is the energy of the Compton-scattered photon, E is the initial photon energy, $m_e c^2$ is the rest energy of the electron, and θ is the scattering angle of the scattered photon.

In the case of the γ rays produced at HIGS, the electron is not at rest and the kinematic relations become more complicated. For a "head-on" collision, Equation 1.2 becomes:

$$E_\gamma = E_\lambda \frac{1 + \beta}{1 + r - (\beta - r)(cos\theta)}, \tag{1.3}$$

where E_γ is the resulting γ-ray energy, E_λ is the energy of the fel photon, $r = E_\lambda / E_e$, and $\beta = v_e/c$, where v_e is the velocity of the electron and c is the speed of light. Sample energy distributions for various DFELL operating parameters are given in Figure 1.3. The energy resolution of the beam used by the experimenter is determined by collimating the beam. Placing a small circular collimator along the optical axis of the γ rays allows γ rays to pass which have an energy spread given by the maximum energy down to a lower energy which is defined by the collimator radius, where the energy distribution is given by Equation 1.3. The energy resolution which is obtained by using Equation 1.3 is the theoretical minimum resolution for the given collimator set-up. The spreading of the electron bunches in energy and momentum worsens this resolution. For example, electrons which are slightly higher or lower in energy

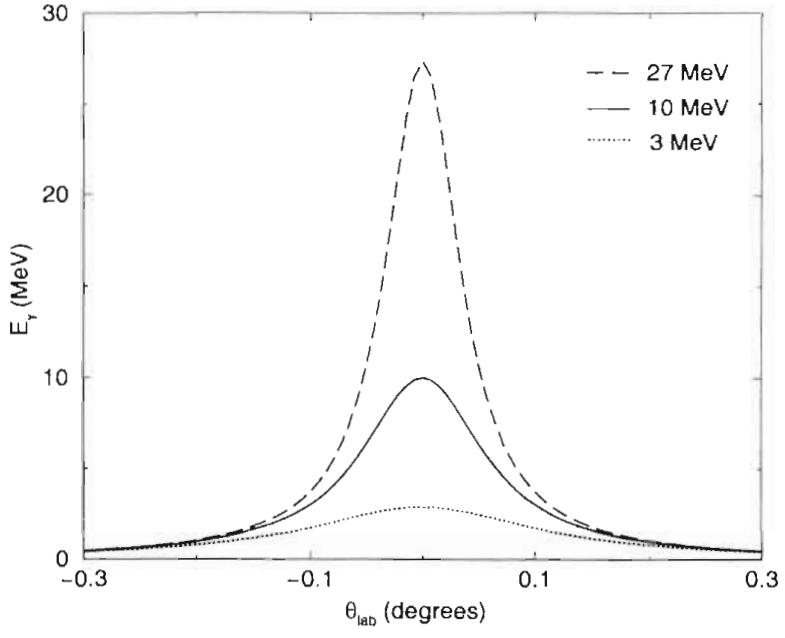

Figure 1.3: Plot of the γ energy as a function of scattering angle. The dashed line (max. $E_\gamma = 27$ MeV) was generated by scattering 750 MeV electrons from 3.296 eV photons. The solid line (max. $E_\gamma = 10$ MeV) was for 450 MeV electrons scattering from 3.296 eV photons. The dotted line (max. $E_\gamma = 2.9$ MeV) was for 240 MeV electrons scattering from 3.296 eV photons.

produce γ rays which are slightly higher or lower in energy, therefore the degree of monochromatization of energy is worsened. Other factors contribute to the intrinsic energy resolution of the γ-ray beam, but they are very small compared to the effect of the electron beam energy spreading.

1.2.4 Flux

The magnitude of the γ-ray flux at DFELL primarily depends on the amount of electrons and fel photons which are available for an interaction. So, naturally, it is desirable to store as much current in the storage ring as possible while keeping the electron beam stable. The goal for obtaining high fluxes is attempting to increase the amount of current stored in the ring since the probability of an interaction with

the fel photons is rather small.

The expression for the scattering cross section when the electrons are not at rest and the initial photons are polarized can be derived using Quantum Electrodynamics and the kinematic invariants s, t, and u. For unpolarized electrons and linearly polarized initial photons (which is the case at DFELL) the cross section in the lab frame for a "head-on" collision is [Lit96]:

$$d\sigma = \frac{8r_e^2}{x^2}\left\{\frac{1}{4}\left(\frac{x}{y}+\frac{y}{x}\right)+(1-cos2\phi)\left[\left(\frac{1}{x}-\frac{1}{y}\right)^2+\left(\frac{1}{x}-\frac{1}{y}\right)\right]\right\}\left(\frac{E_\gamma}{m_ec^2}\right)^2 d\Omega', \quad (1.4)$$

where,

$$x = \frac{2\gamma_{rel}E_\lambda(1+\beta)}{m_ec^2}, \quad (1.5)$$

$$y = \frac{2\gamma_{rel}E_\gamma(1-\beta cos\theta)}{m_ec^2}, \quad (1.6)$$

and ϕ is the azimuthal angle, γ_{rel} is the relativistic factor $\gamma_{rel} = E_\gamma/m_ec^2$, and r_e is the classical electron radius. For the case of photons polarized parallel to the plane of scattering, $\phi = 90°$. In the electron rest frame with unpolarized photons this reduces to the familiar Klein-Nishina formula:

$$d\bar{\sigma} = \frac{r_e^2}{2}\left(\frac{E'_\gamma}{E_\lambda}\right)^2\left\{\frac{E_\lambda}{E'_\gamma}+\frac{E'_\gamma}{E_\lambda}-2sin^2\theta\right\}d\Omega', \quad (1.7)$$

where $d\bar{\sigma}$ is the unpolarized scattering cross section. This simplified version of the cross section will be discussed in more detail in Chapter 2. A plot of Equation 1.4 for various operating parameters is shown in Figure 1.4. Notice that when the γ-ray energy is high, the distribution becomes more forward-peaked. This leads to higher fluxes of γ rays through a given collimator as the γ-ray energy increases.

By knowing the total number of fel photons and electrons which are available for scattering, Equation 1.4 can be used to make an estimate of the expected flux, a

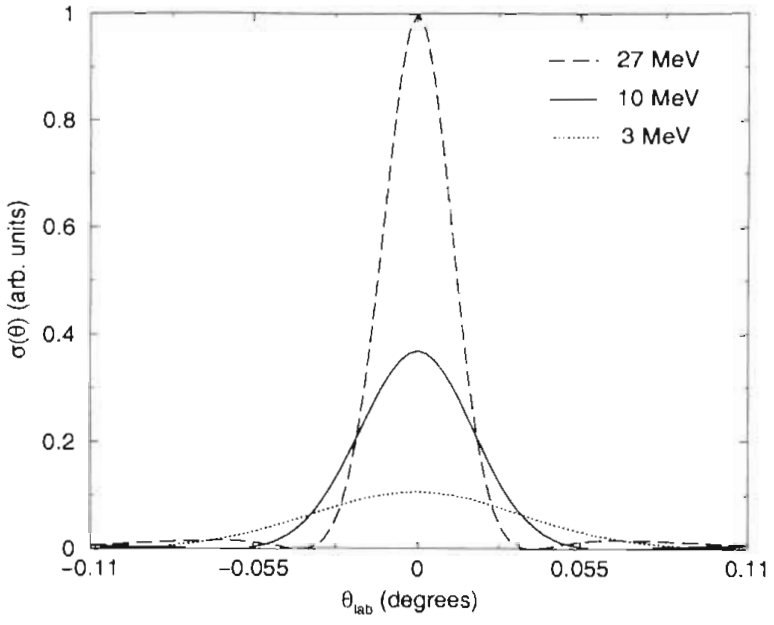

Figure 1.4: Plot of the differential cross section (in arbitrary units) as a function of scattering angle. The dashed line (max. E_γ = 27 MeV) was generated by scattering 750 MeV electrons from 3.296 eV photons. The solid line (max. E_γ = 10 MeV) was for 450 MeV electrons scattering from 3.296 eV photons. The dotted line (max. E_γ = 2.9 MeV) was for 240 MeV electrons scattering from 3.296 eV photons.

detailed description of this can be found in [Par00]. By integrating over $d\Omega'$, the total flux can be calculated. The more useful quantity, however, is the total collimated flux which means only integrating over the solid angle subtended by the small collimator aperture. The percentage of the total flux through the collimator depends on both the geometry of the collimator set-up and the energy of the electrons.

1.3 Alternate Methods for Measuring Flux

Since numerous experiments, including absolute cross section measurements, have been performed at other institutions with photon beams, there must be adequate methods for measuring the flux. Unfortunately the nature of the photon beam at DFELL makes these methods either ineffective or impossible as a means of measuring

the flux. These techniques will be briefly described below.

Photon Tagging Facilities

The majority of photon beams currently being used as a source of γ rays for studies in nuclear physics are photon tagging facilities. These facilities produce their photon beams by producing bremsstrahlung radiation.

In these facilities an electron beam is incident on a radiator foil (usually aluminum), the electrons then slow down in the foil and emit bremsstrahlung radiation at all energies up to the incident kinetic energy of the electrons. The primary electrons which escape the foil without any interaction are swept away from the resulting photon beam using a magnetic field to direct them into a faraday cup. The secondary electrons, which produced the photons, are also swept away by a magnetic field into a magnetic spectrometer. These electrons are momentum analyzed by sweeping them into a focal plane of many small plastic scintillators. By "tagging" the photons observed in a γ-ray detector in coincidence with a secondary electron detected in one of the scintillators, both the energy and flux of the photons can be determined. The photon tagging facility at the Saskatchewan Accelerator Laboratory (SAL) shown in Figure 1.5 typically sees $4x10^6$ γ/sec/MeV with an energy resolution of 1% over the tagged photon energy range of 30-210 MeV [Iga01]. This type of facility is capable of measuring the flux with only 1% uncertainty.

Pair Spectrometer

A pair spectrometer operates under similar principles as a photon tagging facility. With a pair spectrometer, a photon beam is incident on a converter foil in order to produce electron/positron pairs. These pairs then enter a magnetic spectrometer with scintillating detectors similar to that of a photon tagging facility. In this case,

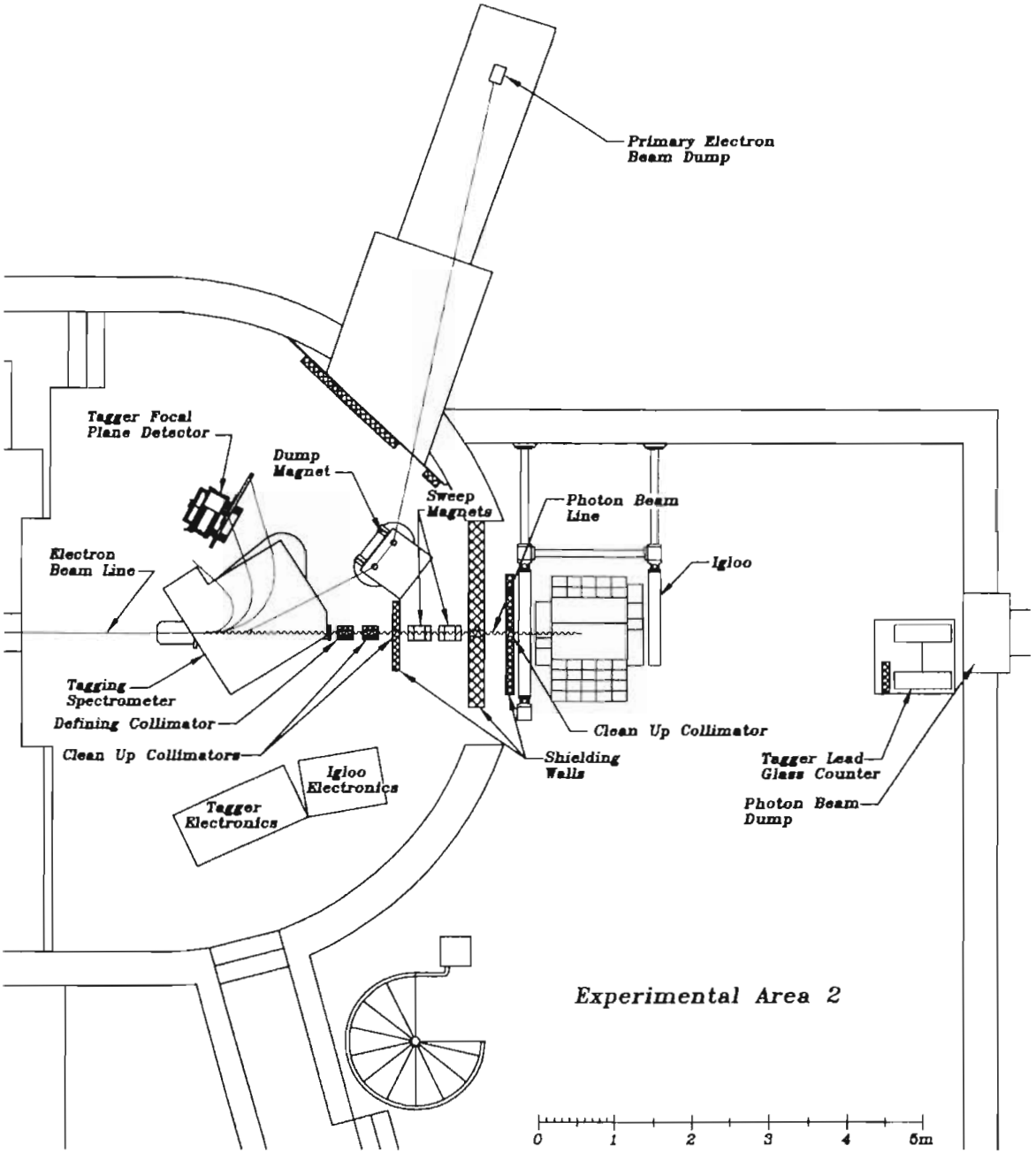

Figure 1.5: Photon tagging facility at the Saskatchewan Accelerator Lab. Figure taken from [Vog95].

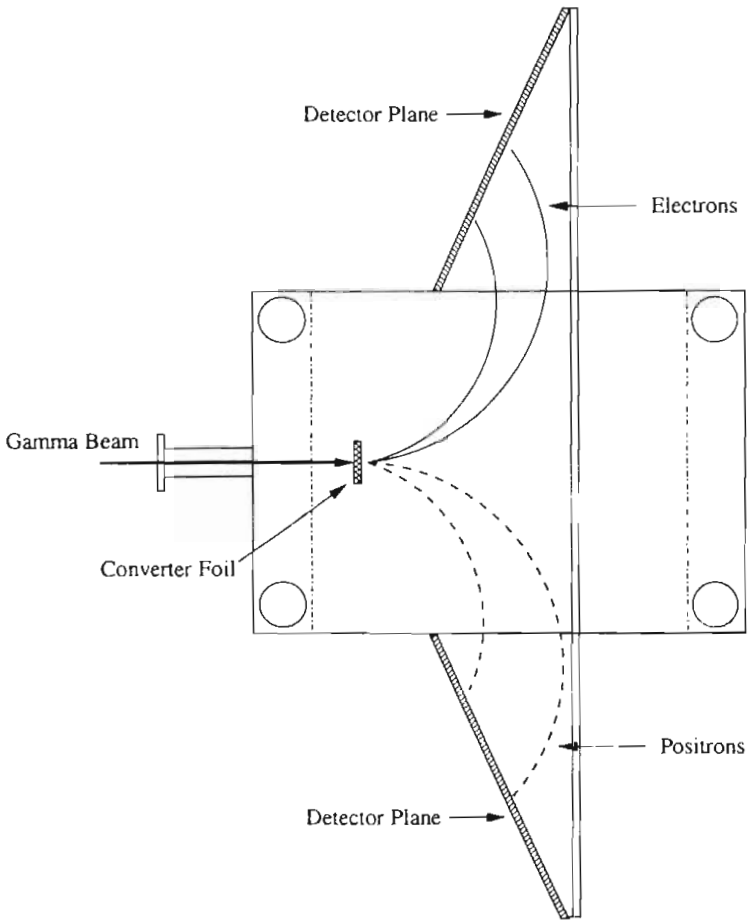

Figure 1.6: Schematic diagram of a pair spectrometer.

the electrons are swept in one direction into a focal plane of scintillators, while the positrons are swept to the opposite direction into another focal plane of scintillators. The pairs are then momentum analyzed, and, if the conversion rate of the foil is well known, the incident flux of the γ rays can be determined. Since the pair spectrometer depends on the production of electron/positron pairs, it is not very useful for measuring fluxes at low energies where Compton scattering and the photoelectric effect play a large role in the photon attenuation in the converter foil. Also, once the pairs are produced they can undergo radiative and collision losses. Therefore it

is useful to have as thin a foil as possible, which requires very high fluxes to make a measurement. An attempt to measure the flux at HIGS was done by Eric Schreiber [Sch00] using a pair spectrometer (Figure 1.6) from the Saskatchewan Accelerator Laboratory (SAL). For the above reasons and poor energy resolution of the detector system it proved to be inadequate as a flux monitor for the current operating capabilites at HIGS. In the future, there are plans to replace the detectors in the focal plane with much smaller detectors to increase the energy resolution.

Measuring Optical Cavity Power and Beam Current

In theory, since the physics behind Compton scattering is so well understood, the flux can be calculated with adequate accuracy by knowing the number of photons and electrons available for scattering, and the angular and energy spread of the respective bunches. Therefore it is possible to calculate the estimated flux of the γ-ray beam with a measure of the power in the optical cavity and the current in the storage ring. This is accomplished by measuring the power through a CaF_2 output window in the optical cavity and then simply accounting for the transparency of the window, which is usually known. The major problem with this method is that it is only accurate to 10-20% as a measure of the flux. This uncertainty mainly comes from the uncertainty in knowing how the photon bunch and electron bunch overlap at the collision point. For instance, the electron beam can be slightly misaligned, or the optical axis of the photon beam can shift due to small thermal stresses on the mirrors. In normal operating mode, both of these parameters are "played with" until the flux is maximized, but this does not necessarily correspond to a perfect "head-on" collision of the photons and electrons. Unless the uncertainty in how they collide is reduced, this method will not have sufficient accuracy as a measure of the flux.

Direct Measurement

The most direct and accurate measure of the flux is accomplished by placing a sodium iodide γ-ray detector directly in the beam and then simply counting the number of γ rays detected. (The physics of sodium iodide detectors will be discussed in more detail in the Section 2.3.1.) Once the efficiency of the detector is known, it is straightforward to calculate the flux to an accuracy of 1% assuming you can get the efficiency to this or better accuracy - which is not trivial. The major problem with this method is that these detectors have a very low maximum counting rate (10^4 Hz) and therefore become unreliable for incident fluxes which are higher than this, which is the case at HIGS. One remedy for this problem is to first attenuate the γ beam with a high Z material, e.g. lead or iron. This reduces the γ flux incident on the detector, but it often requires several inches of attenuating material which introduces unwanted uncertainty into the measurement, such as the spreading of the γ-ray peak and an increase in the background underneath the peak. Another reason that this method is not ideal is because placing such large objects as a detector and several inches of lead directly into the γ-ray beam introduces a lot of background radiation that can interfere with the actual experiment being performed.

1.4 Motivation

The HIGS nuclear physics program at the Duke Free-Electron Laser Laboratory will provide a testing ground for certain aspects of photonuclear physics which will be unmatched by any other institution in the world. With its current operating parameters, experiments done by Eric Schreiber [Sch00] have provided a solid starting point for the exciting future of the HIGS program, and with upgrades which are soon to be completed the future will only be brighter.

All future experiments at HIGS which use the γ-ray beam will need to accurately

know the flux and a sound technique for this measurement must be developed. Most experiments which will be performed at HIGS will be technically challenging, therefore this flux measurement should be as simple as possible so as to not take the experimenter's attention away from the main experiment.

Other institutions which provide photon beams have had success in measuring the γ-ray fluxes, however their techniques are ineffective or inapplicable due to the unique nature of the HIGS γ-ray beam and how it is produced. The most simple techniques, such as direct measurement with a γ detector or a measurement of the power in the optical cavity, are inadequate and a more creative solution must be found.

Chapter 2

Experimental Methods

2.1 Overview

The Compton scattering of γ rays from electrons is a very well understood phenomena in physics. In this work, γ rays which were Compton-scattered at a small angle with respect to the incident beam from a target of known density and thickness were used to determine the incident γ-ray flux. The Klein-Nishina formula for the differential scattering cross section of the Compton-scattering process gives an exact description of this process and, in principle, can be used to predict the observed counting rates.

2.1.1 Basic Set-up

The basic idea behind this technique is to detect γ rays at fluxes which are low in comparison to the direct flux of the beam (10^2-10^3 γ/sec) and are therefore more manageable for the detector and the data acquisition system. Therefore, rather than place a detector in the beam, a thin scattering target is placed in the beam and a detector is placed at some angle from the beam axis to detect the scattered radiation. This target serves as an electron target which Compton scatters the γ rays according to the well-known Klein-Nishina relation. The incident flux of these scattered γ rays on the off-axis detector is 3-4 orders of magnitude lower than the primary flux. The total γ-ray flux of the beam can then be deduced according to the probability distribution for Compton scattered photons.

Concurrent with this measurement, another NaI detector was placed directly in the beam to make a direct measurement, and the deduced fluxes were then compared. This direct measurement was done using a low total incident beam intensity (10^5

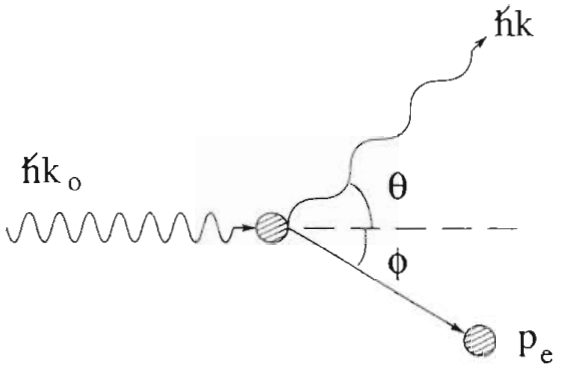

Figure 2.1: Compton scattering in which the electron is at rest.

γ/sec) so that a direct measurement was possible. With the in-beam detector and the off-axis detector in place, a systematic experiment was performed with two main parameters being varied in our measurements: the target thickness and the angle of the off-axis detector.

2.1.2 Kinematics

In Compton scattering, a photon is incident on a free electron and there is a "billiard-ball" collision. A schematic diagram for this type of collision in the electron rest frame is shown in Figure 2.1. Applying conservation of momentum gives:

$$\hbar k sin\theta = p_e sin\phi, \tag{2.1}$$

$$\hbar k_\circ = \hbar k cos\theta + p_e cos\phi, \tag{2.2}$$

where $\mathbf{k}_\circ$ is the initial photon wave vector, $\mathbf{k}$ is the final photon wave vector, and $\mathbf{p_e}$ is the final momentum of the electron. Applying conservation of energy gives:

$$\hbar\omega_\circ + m_e c^2 = \hbar\omega + \sqrt{m_e^2 c^4 + p_e^2 c^2}. \tag{2.3}$$

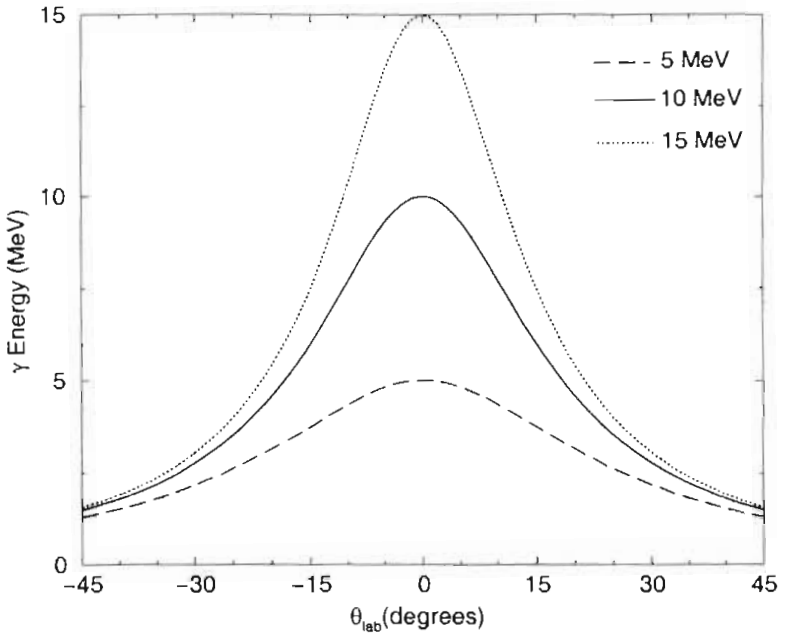

Figure 2.2: Energy of γ rays Compton-scattered from an electron at rest as a function of angle. This is a plot of Equation 2.4.

Using both of these results, the energy distribution of the Compton scattered photons is obtained:

$$\hbar\omega = \frac{\hbar\omega_0}{1 + \frac{\hbar\omega_0}{m_e c^2}(1 - cos\theta)}. \tag{2.4}$$

This is Equation 1.3 with the approximation that $v_e << c$, which is the case for the electrons in the scattering target. A plot of Equation 2.4 is given in Figure 2.2 for various incident γ-ray energies.

2.1.3 Scattering Cross Section

When Compton originally determined an expression for the cross section for Compton scattered photons, it was for scattering from a spinless particle. Many years later, after the development of QED, Klein and Nishina improved on this by applying Dirac's relativistic theory of the electron, where the electron can exist in four possible

states: two spins states and having either positive or negative energy. The relation derived by Klein and Nishina was given by Equation 1.7, however this does not take the polarization of the photons into account. The γ rays incident on the scattering target are 100% linearly polarized.

The Klein-Nishina formula for the differential scattering cross section for linearly polarized photons scattered from electrons is [Eva55]:

$$\frac{d\sigma}{d\Omega} = r_e^2\Big[\frac{1}{1+\alpha(1-cos\theta)}\Big]^2\Big\{sin^2\xi + \frac{\alpha^2(1-cos\theta)^2}{2[1+\alpha(1-cos\theta)]}\Big\}, \tag{2.5}$$

where $\alpha = \frac{\hbar\omega}{m_e c^2}$, θ is the angle of the scattered photon in the lab frame, and ξ is the angle between the electric field vector of the incident photon and the scattering angle of the scattered photon. Equation 2.5 has been summed over all possible directions of polarization for the scattered photon, since the final polarization is not important to this measurement. It is useful to use the following relation for ξ:

$$sin^2\xi = 1 - sin^2\theta cos^2\eta, \tag{2.6}$$

where η is the angle between the plane of polarization and the scattering plane. Therefore the probability for a photon to be scattered perpendicular to the polarization plane ($\eta = 90°$) is greater than being scattering in the parallel plane ($\eta = 0°$). Although the cross section is slightly higher with $\eta = 90°$, the γ detector was located in the parallel plane due to physical limitations. Since all of the photons at HIGS are, currently, linearly polarized with the electric field vector parallel with the scattering plane of the γ detector, $\eta = 0°$ for all of the measurements and the $sin^2\xi$ then reduces to $cos^2\theta$. Equation 2.5 can then be written completely in terms of the scattering angle θ,

$$\frac{d\sigma}{d\Omega} = r_e^2\Big[\frac{1}{1+\alpha(1-cos\theta)}\Big]^2\Big\{cos^2\theta + \frac{\alpha^2(1-cos\theta)^2}{2[1+\alpha(1-cos\theta)]}\Big\}. \tag{2.7}$$

A plot of Equation 2.7 for various incident photon energies is shown in Figure 2.3.

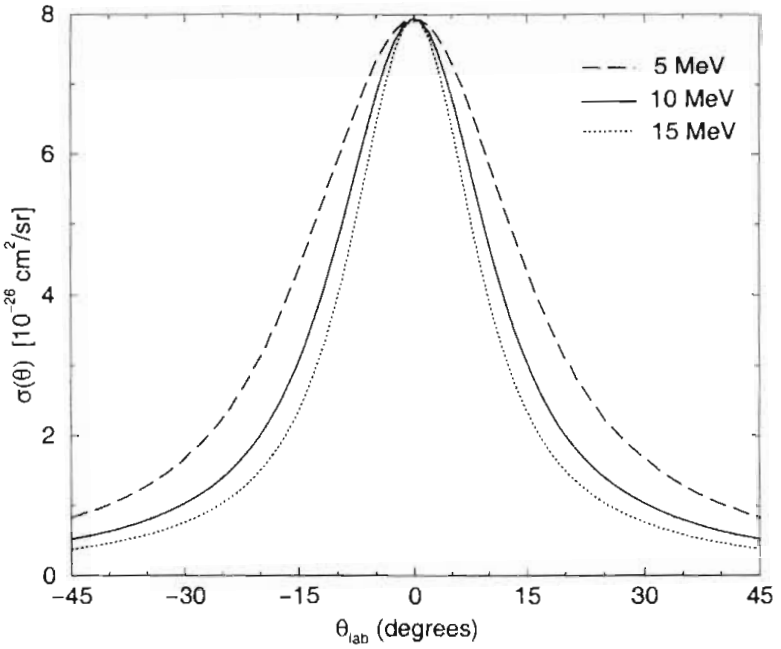

Figure 2.3: Differential cross section as a function of scattering angle for γ rays scattered by electrons at rest. The dashed line represents 5 MeV γ rays, the solid line represents 10 MeV, and the dotted line is 15 MeV.

2.2 Experimental Set-up Parameters

A diagram of the set-up is given in Figure 2.4. The details of the set-up are discussed below, as well as the rationale for many aspects of the set-up.

2.2.1 Collimation

Determining the collimation of the beam is one of the most important aspects of any experiment at HIGS since it geometrically limits the energy resolution and flux of the beam. The collimator used in this experiment was a 1" diameter iron collimator which was 6" in length. This was chosen for several reasons. First, a large flux through the collimator was desired and, at energies between 10-15 MeV, a large percentage of the flux passes through while still providing a well-defined beam. A 1" collimator will let

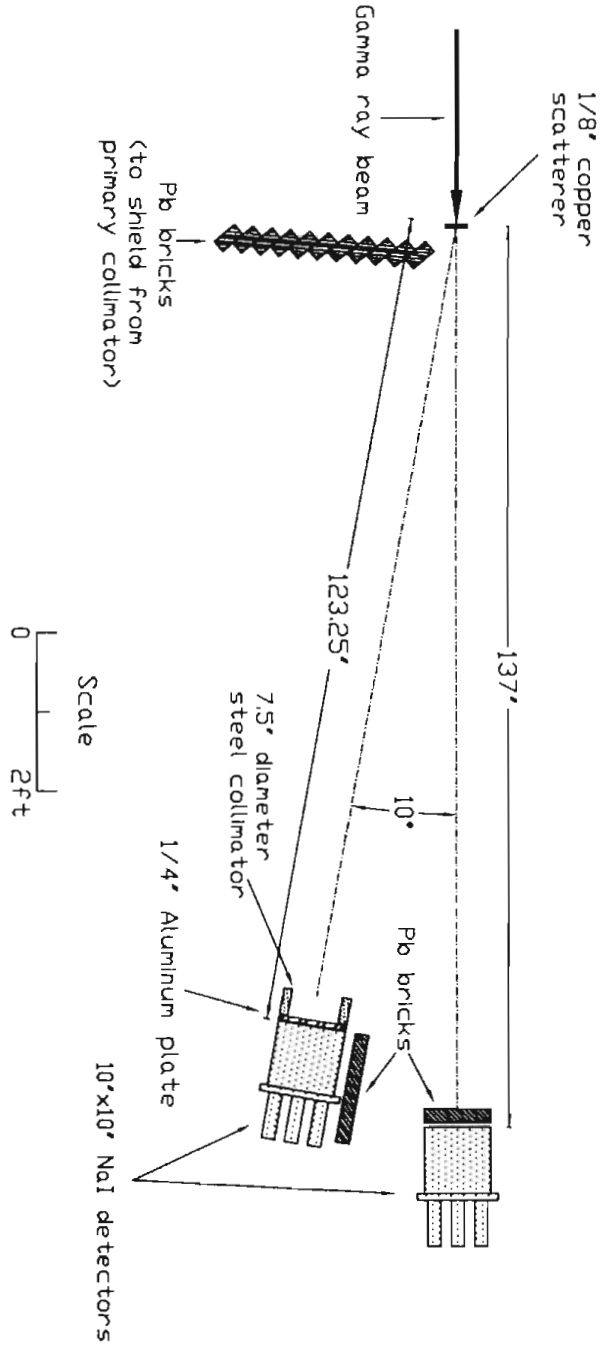

Figure 2.4: Experimental set-up for the Compton scattering experiment. This diagram shows a top view and all the units are in inches. Not included in this picture are the primary collimator or the beam dump.

a beam through with approximately 3.5% resolution at 10 MeV; this is approximately equal to the resolution of the NaI detectors at this energy. Reducing the size of the primary collimator would give better beam resolution, but it would also lower the flux which, for this experiment, was undesirable.

In addition to collimating the beam, the collimator also, unfortunately and unavoidably, serves as a source of background radiation, the most important of which being neutron production. The photoproduction of neutrons has a very high cross section at 17 MeV for most materials, but it is higher for materials with a high Z, such as lead, rather than lower Z materials such as copper. Even though high Z materials readily produce neutrons, they also attenuate γ rays very well. This experiment was performed at γ-ray energies of 10 MeV and 15 MeV, and 10 MeV is below the neutron production threshold energy for iron (which is at 11.2 MeV). Therefore, at 10 MeV, no neutrons would be produced by an iron collimator and very few would be produced at 15 MeV. At the same time, the iron attenuated approximately 97% of the incident γ rays. One alternative to iron is lead, which would produce neutrons at 10 MeV and increase the neutron production approximately 7 fold at 15 MeV, however a lead collimator would attenuate approximately 99.98% of the incident γ rays. So, for neutron suppression reasons, iron seemed to be the choice for the collimator material. With the recent construction of a new concrete hut at DFELL to house the primary collimator, this neutron suppression will be much less of an issue. The experimental area is now well-shielded from the primary collimator so that lead collimators can be used, which will be a huge improvement for future experiments.

2.2.2 Scattering Targets

Various types of scattering targets were tested in this experiment, varying in material and thickness. The considerations that went into determining the scattering target

were effective target thickness, neutron production, and γ-ray attenuation. The effective target thickness (N) is the number of electrons per square centimeter, which is given by the following relation:

$$N = \frac{Z}{A}\rho N_a x, \tag{2.8}$$

where Z is the atomic number, A is the atomic mass, ρ is the mass density, N_a is Avogadro's number, and x is the actual thickness of the target. The effective target thicknesses for various materials are given in Appendix B.

A major concern in considering possible scattering targets is the neutron production discussed earlier. The cross sections for the photoproduction of neutrons are determined very well and can be found in [Die88]. Since this experiment was performed at 10 and 15 MeV, copper was chosen since it has a high electron density and it produces very little neutrons at these energies. Lead targets were also tested to see the effect of the neutron contribution.

The last consideration was the attenuation of the γ rays by the scattering target. Having a thick target meant having more electrons available for scattering, however it also means that the amount of attenuation is increased. So a scattering target should be thick enough to provide a decent count rate in the off-axis detector, but should also be thin to minimize the attenuation of the beam. In order to find an ideal thickness, it is necessary to take a closer look at the attenuation process. At the energies for this experiment, the two dominant processes that went into attenuating the γ rays were Compton scattering and pair production. The attenuation due to Compton scattering is proportional to Z, while for pair production it is proportional to Z^2. Since Compton scattering is the process of interest, we would like the attenuation due to this process to be large, while the pair production should be kept to a minimum. The best materials under these guidelines are medium to low Z materials, such as nickel, copper, and iron. The effective target thicknesses and attenuation for various

Material	Target Thickness $[10^{23}$ e$^-$/cm$^2]$	$e^{-\mu x}$ (10 MeV)	$e^{-\mu x}$ (15 MeV)
1/4" Cu	15.64	0.8383	0.8312
1/8" Cu	7.820	0.9156	0.9117
1/8" Pb	8.585	0.8362	0.8156
1/16" Pb	4.293	0.9144	0.9031
1 cm Al	7.831	0.9398	0.9431

Table 2.1: Target thicknesses and attenuation for various materials and thicknesses. The values in the $e^{-\mu x}$ columns are the amount of transmission, for example a 1/4" Cu target will transmit 83.83% of an incident γ-ray flux of 10 MeV γ rays.

materials are given in Table 2.1. The actual effective target thicknesses for the targets used in this work are given in Appendix A.

2.2.3 Shielding Concerns

The main sources of background radiation are the collimator, the scattering target, beam dump, natural room background, and anything that needed to be placed directly in the γ-ray beam (such as lead attenuators and a NaI detector for in-beam measurements). To get the cleanest spectrum of the scattered γ rays from the target, these backgrounds had to be suppressed as much as possible.

Since the count rate was expected to be much lower in the off-axis NaI detector, greater efforts were made to properly shield this detector rather than the in-beam NaI. The primary shielding concern for the off-axis detector was shielding from the collimator. The collimator served as a source of low energy γ rays and low energy charged particles. To shield from this radiation, an approximately 4" thick wall of lead bricks was placed in between the detector and the collimator so that there was no direct line of sight between the two. It was also necessary to shield the off-axis NaI from the in-beam NaI and the lead wall which attenuated it. Therefore a 2" thick wall of lead was placed along the side of the off-axis NaI. Both of these lead

walls are shown in Figure 2.4. It was not deemed necessary to shield the back of the off-axis NaI from the beam dump since there was no line of sight to the back of the beam dump, even at the smallest angles.

Another shielding concern was the radiation from the scattering target. Most of this radiation was γ rays, electrons from Compton scattering, and electrons and positrons from pair-production occuring inside the target. Obviously it was not desirable to shield from all of this radiation since detecting the Compton-scattered γ rays is the entire point of this experiment. Therefore a thin (1 cm) aluminum plate was placed over the face of the detector. Since aluminum has a low Z it will not attentuate γ rays very much (as seen in Table 2.1), while it would stop many of the electrons. Figure 2.5 shows the effect of the aluminum plate in stopping some of the low energy charged particles. A much better solution to shielding from these charged particles would have been to have replaced the aluminum plate with a thin plastic scintillator to serve as a charged-particle veto counter. However a plastic scintillator large enough for this purpose was not available at the time of the experiment. Plastic scintillators will be discussed in more detail in Section 2.3.2.

Cosmic rays were not considered to be a major problem in this experiment. At energies of 10 MeV and higher, cosmic rays play the most important role in natural background radiation and are usually rejected by surrounding the detector in a plastic anti-coincidence shield. In this experiment, however, a signal from the RF cavity in the storage ring was used to "time-gate" the off-axis NaI. Using this signal, most of the random background radiation was rejected. This procedure of using the RF pulse will be discussed in much more detail in Section 2.4.

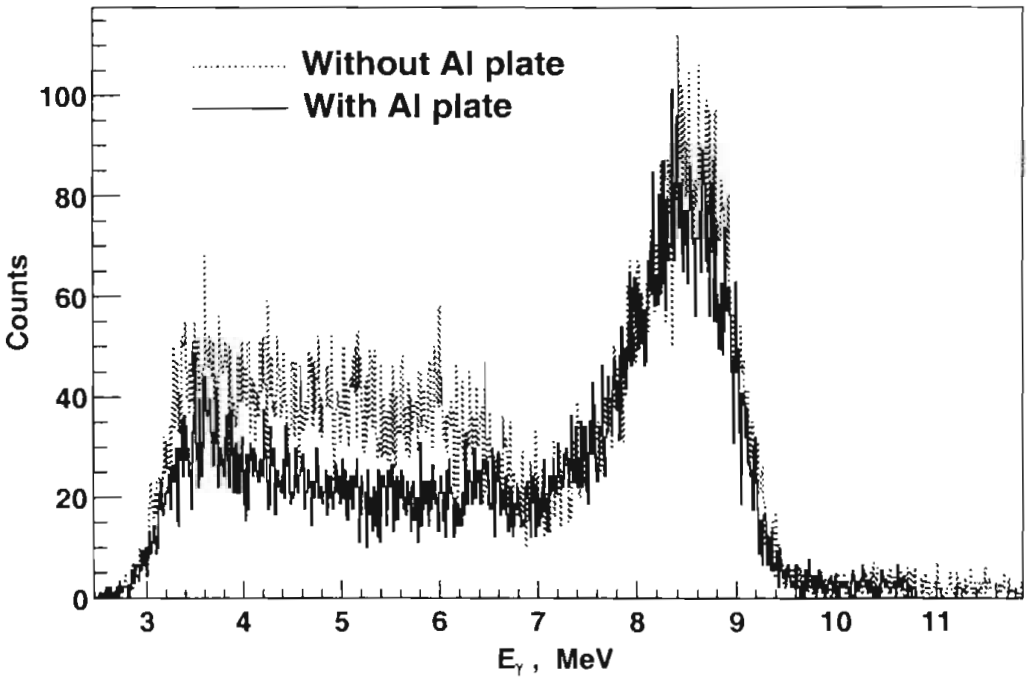

Figure 2.5: Spectra showing the effect of placing a 1 cm aluminum plate in front of the off-axis detector. The dotted line is without the aluminum plate and the solid line is with the plate. This spectra is for 10 MeV γ rays scattering at 5° from a 1/4" Cu scatterer. The count rate in these peaks have been normalized.

2.2.4 Detector Placement

The most important factor that goes into the placement of the off-axis NaI detector is trying to attain an appropriate count rate in the detector. Other factors include minimizing the energy spread of the γ rays incident on the detector, minimizing background, and the physical limitations on the position.

Figure 2.3 shows that the differential cross section falls off with angle more rapidly as the energy of the γ rays increases. For a given incident flux and target thickness, to maintain a certain count rate in the detector means maintaining a certain differential cross section in the solid angle subtended by the detector. So at low incident fluxes (10^5 γ/sec) the off-axis detector must be placed at a small angle, while at higher

fluxes (10^7 γ/sec) the detector could be placed at a larger angle. An additional motivation behind moving to larger angles is to move the detector further away from any possible background radiation from the scattering target or the beam dump. The other approach explored in this experiment was to keep the detector at a fixed angle and then vary the thickness of the scatterer, where a thin foil would be used for high fluxes and a thicker target would be used for low fluxes. In designing this experiment, one of the goals was to determine what an acceptable count rate in the off-axis detector actually was, therefore many different situations were tested.

2.3 Detection System

NaI detectors have a decent energy resolution and a very high detection efficiency for the range of γ-ray energies present in this experiment. Other detectors such as High-Purity Germanium detectors have a much better energy resolution but poor efficiency, while the reverse is true for detectors such as Pb-glass detectors. Because of the balanced qualities of the NaI detectors, they were chosen as the primary detectors for this experiment.

2.3.1 NaI Detectors

A NaI detector consists of a large NaI crystal (which is an inorganic scintillating crystal) encased in a very thin aluminum casing. One side of the crystal is optically coupled to several photomultiplier tubes which detect the scintillated radiation and convert it to an electrical pulse whose size can be related to the energy of the incident γ-ray.

The characteristics of NaI detectors can be explained by looking at how the γ rays are actually detected. There are three important interactions between photons and matter which can come into play: the photoelectric effect, Compton scattering, and

pair production. Through these interactions the γ-ray deposits some of its energy into the crystal. If exactly all of the energy is perfectly deposited in the detector there would be a sharp peak (the photopeak); instead there is a broad peak whose shape is well-understood and is referred to as the "response function" of the detector. A typical spectrum of the response function is shown in Figure 2.6. It is possible for a γ-ray to interact with the crystal via Compton scattering which produces a lower energy γ-ray. If this γ-ray escapes the crystal, only a fraction of the initial γ-ray energy is deposited. This contributes to a low energy tail in the response function, with a leading edge called the "Compton edge". Another contribution to the response function are the escape peaks from pair production. When a γ-ray is converted to an electron and a positron, the positron slows down via atomic ionization and bremsstrahlung. Once thermalized, it has a large cross section for pair annihilation whereby it is converted into two 511 keV photons. If one or both of these γ rays escape the detector before depositing their energy, the energy deposited is the full energy minus 0.511 MeV or 1.022 MeV, respectively. At 10 MeV, the resolution of the NaI detector is too large to resolve these escape peaks or the Compton edge and what is left is the broad response function. The full-width at half-maximum divided by the peak energy is defined as the resolution of the detector. A typical resolution for a 10"x10" NaI detector is 3-4% at 10 MeV.

It is desirable to have as many of the initial γ rays deposit their full energy as possible. There are two main factors that go into this: the size of the detector and the material of the crystal. First, with a large crystal the probability of depositing the full amount of energy increases. Therefore the largest NaI detector available was used, which was a 10"x10" crystal. The other factor was the material of the crystal. The high Z of NaI means that pair production is a large contribution to the total interaction cross section at these energies. This increases the photopeak efficiency

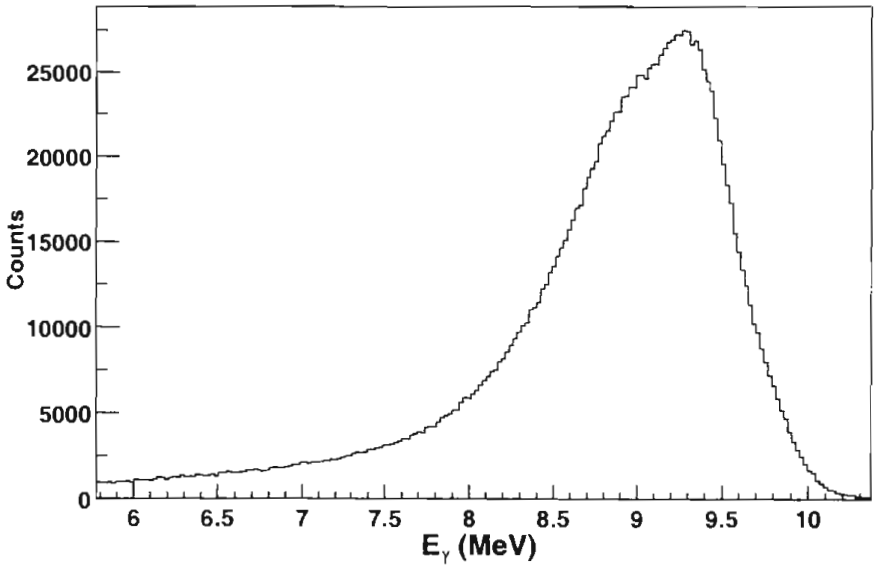

Figure 2.6: Experimentally determined response function of 10" x 10" NaI detector with an incident γ-ray energy of 10 MeV. This was after being attenuated by 2" of lead, which broadened the peak significantly.

with respect to the Compton distribution.

The efficiency of the NaI detector has a conventional definition. Once the full-width at half-max of the response function is extracted, the response function is integrated over the range determined as two full widths below the centroid to one full width above the centroid. The efficiency is then this integral divided by the integral of the entire response function. The efficiency for this detector is approximately 57%, which is relatively high.

Several photomultiplier tubes are optically coupled to the crystal in order to convert the low energy photons from the scintillating crystal into electrical pulses. In a photomultiplier tube, the photons are incident on a photo-sensitive cathode which then emits photoelectric electrons. These electrons are then accelerated through an array of dynodes which greatly amplifies the electrical pulse. The pulse is then carried by a low-loss cable to the electronics for analysis.

2.3.2 The Best of the Rest

Several other types of detectors were used in this experiment, but they were all of secondary importance so the discussion of their operating characteristics will be limited. The other detectors were a plastic scintillating detector and a Pb-glass detector.

Plastic Scintillator

A plastic scintillator operates in a similar way to the NaI detector, in that they are both scintillating materials which are optically coupled to a photomultiplier tube. Plastic scintillators are organic scintillators which produce very fast pulses (several nanoseconds). This makes them very useful as counters for situations in which the only information of interest is whether or not a high-energy charged particle or γ-ray passed through the scintillator. It was in this capacity that a plastic scintillator was used in this experiment. A thin (0.5 cm) plastic scintillator was placed directly after the primary collimator and counted the γ rays which passed through with a detection efficiency of roughly 2% for γ rays at these energies. This counter could not serve as a reliable γ-ray counter, however, since it also counts high-energy electrons and positrons with nearly 100% efficiency without distinguishing them from γ rays. Therefore charged particles coming from the collimator are incorrectly counted as γ rays. Despite these problems, the counting rate of the plastic scintillator served as a good reference point when comparing the fluxes seen by both NaI detectors.

Pb-Glass Detector

A Pb-Glass detector was placed at the end of the beam dump in the experimental area. It was used in a similar manner as the plastic scintillator, in that it was simply a γ-ray counter. A Pb-glass detector operates in a similar manner as the NaI detectors,

except that its Z is much higher and is therefore nearly 100% efficient at detecting γ rays at 10 and 15 MeV. Unfortunately it has horrendous energy resolution at these energies and could only serve as an approximate beam intensity monitor. The Pb-glass detector used in this experiment was one of the detectors used in a neutral pion spectrometer (Igloo) at the Saskatchewan Accelerator Lab (SAL) [Vog95]. It has a 19.1 cm x 19.1 cm square cross section and is 30.5 cm long. Since this detector was a new detector for this facility, a preliminary study was done to see how well the detector behaved under such intense γ-ray fluxes, and to get a rough idea of the actual detection efficiency.

2.4 Electronics

The electronics in this experiment serve to amplify and discriminate the analog signal coming from the detector, as well as to convert these signals to a digital format which can be read into the computer-based data acquisition system for analysis.

The NaI detectors used in this experiment had several photomultiplier tubes attached to the crystal. The analog signals from these tubes were gain-matched and then joined together. This composite signal was then attached to a clipping line, which is a long (~50ft) coaxial cable terminated by a variable resistor. This served to reflect an inverted and delayed copy of the original signal whose size was adjusted by the variable resistor so as to cancel the "tail" of the signal, thereby limiting the duration of the pulse to the round-trip transit time of the signal. This technique eliminates the unimportant tail of the signal.

Both NaI detectors had the same basic electronics set-up, with a few modifications which were specific to the individual detectors. The signals were first fanned out with a linear fan module. One copy was sent through a Timing Filter Amplifier (TFA) which amplified the pulse and gave it a shape with a short rise and decay time. This

signal was then sent through a Constant Fraction Discriminator (CFD) which passed only those signals which were above a certain threshold set by the experimenter. One copy of this signal was used as a scaler, while the other was sent to two Gate and Delay Generators (GDG). One of these modules generated a short logic gate (~400 ns) while the other generated a longer logic gate (10 μs). The length and delay of the short gate was set to encompass the amplified energy signal. This short logic gate then served as a trigger for a linear gate. A linear gate is a module which only allows a signal to pass when there is a second coincidence signal present, which is the short logic gate. The purpose of the linear gate is to prevent signals which are below the threshold set in the discriminator from being passed into the Spectroscopy Amplifier. Since the timing signals which generate discriminator pulses are only 10 nsec long, this procedure eliminates pile-up of events below threshold on this time scale. The Spectroscopy Amplifier shapes and amplifies the pulse, so that it is in a form which can be processed by an Analog-to-Digital Converter (ADC), which converts the analog output of the Spectroscopy Amplifier to a digital signal which can be input into a computer. The long gate, from the second GDG described earlier, served as a gate for the ADC. Since it takes the ADC several μs to digitize the signal, a long gate is used to trigger the ADC so that no other signals can reach the ADC before it has finished digitizing the first signal.

The process of inhibiting the ADC so that it can properly digitize signals means that some signals which correspond to real γ rays are never digitized and therefore never show up in the energy spectrum. When making flux measurements, these "missed" γ rays must be taken into account. This is accomplished by making a "dead time" correction. To account for signals which were not digitized as an event, another module called a "hit register" is used which simply counts (using a scaler) the number of pulses produced by the CFD without registering any other information

about the signal, such as pulse height. The "dead time" correction is the the number of scaler events divided by the number of events actually stored.

There was a slight addition to the electronics for the in-beam NaI detector, which are shown in Figure 2.7. When the γ-ray fluxes become higher than $10^6\gamma$/sec, the dead-time corrections are expected to start to become unreliable. Therefore, to avoid problematic dead-time corrections in the future, a second scaler was set-up for this detector to see if it could provide an accurate count rate for the γ rays which was dead-time free.. The energy signal from the Spectroscopy Amplifier was sent to a Single Channel Analyzer (SCA), and the output of this module generated the new scaler. This module essentially has a variable upper and lower threshold which are set by the experimenter. It was set so that the only signals which passed through this threshold window were those signals that corresponded to the "one-width up/two-widths down" convention for the detector efficiency discussed in Section 2.3.1. This will hopefully eliminate dead time problems in the future since the scaler is able to count at a fast rate (10 MHz) without losing any events.

An addition which was made to the off-axis NaI's electronics (shown in Figure 2.8) was a timing gate using the pulse from the RF cavity in the storage ring. For this experiment, the γ-ray production mode at HIGS used two electron bunches in the storage ring. The storage ring operates at a frequency of 2.79 MHz. In one-bunch mode, this means that an electron bunch enters the wiggler every 358 ns, in two-bunch mode it becomes every 179 ns. Therefore γ rays produced by different electron bunches will be 179 ns apart and have a duration of about 200 psec. This timing structure can be exploited in such a way as to produce a spectrum which is only generated by signals which are seen in the detector during the time interval when the γ-ray pulse is present. All other signals which don't have the same time structure as the electron bunches in the storage ring are therefore rejected. This

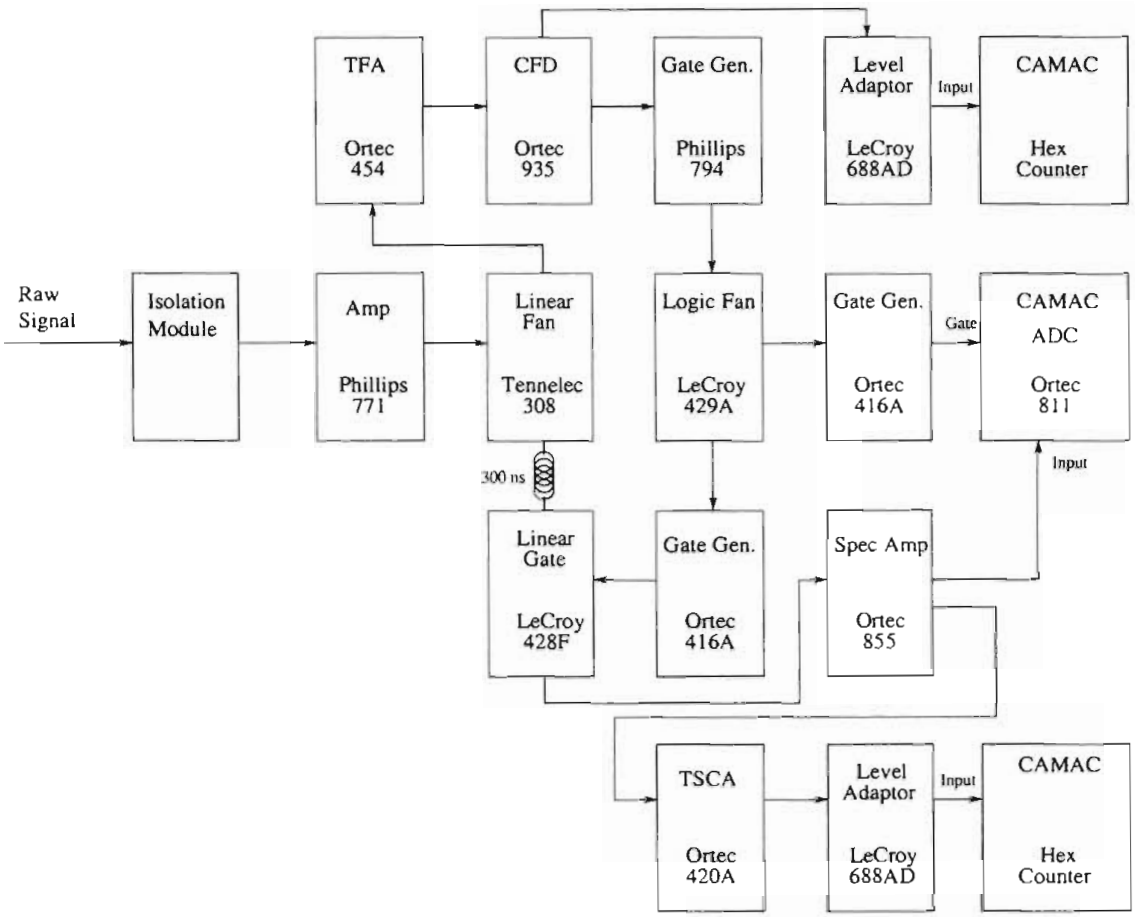

Figure 2.7: Electronics set-up for the in-beam NaI detector.

means that much of the natural background radiation, which is randomly emitted, is rejected, except for a small amount which happen to coincidentally arrive at the detector during this timing window. Since the RF cavity fires every time an electron bunch enters, it must be exactly synchronized with the γ rays. A signal was then pulled out of the RF cavity and this was the signal used to generate the timing-gate.

The first step was to turn the RF signal into a logic signal. This was accomplished by first putting the signal through a "Sum and Invert" module. This module basically inverted the signal to a negative signal which is required for the input to the discriminator. To generate the logic pulse, the signal was passed through a leading edge discriminator, which was triggered by the leading edge of the RF signal (this is shown in Figure 2.9). This generated a series of logic pulses separated by 358 ns, corresponding to one electron bunch. Therefore a second logic pulse, corresponding to the other electron bunch, was needed. To accomplish this, prior to being discriminated, the RF signal was fanned out through a linear fan. Both copies of the signal were each discriminated, producing two identical logic pulses. One of these logic pulses was then delayed so that it occurred 179 ns after the first.

These two pulses were OR'd together in a logic unit and then sent to a Time-to-Amplitude Converter (TAC). A TAC is a module that generates a pulse whose height is determined by the time between two logic pulses, one logic pulse acting as a "START" while the other acting as a "STOP". Since the count rate was expected to be lower in the off-axis NaI rather than the RF pulse, the "START" in this experiment was the off-axis NaI, while the "STOP" was the RF signal. The output of the TAC was then digitized by an ADC. The spectrum produced was the number of events versus the time in which the event occured relative to the RF pulse. Most of the events in the off-axis detector were beam-related, therefore a very narrow peak appeared in the TAC spectrum. An example of this spectrum is shown in Figure

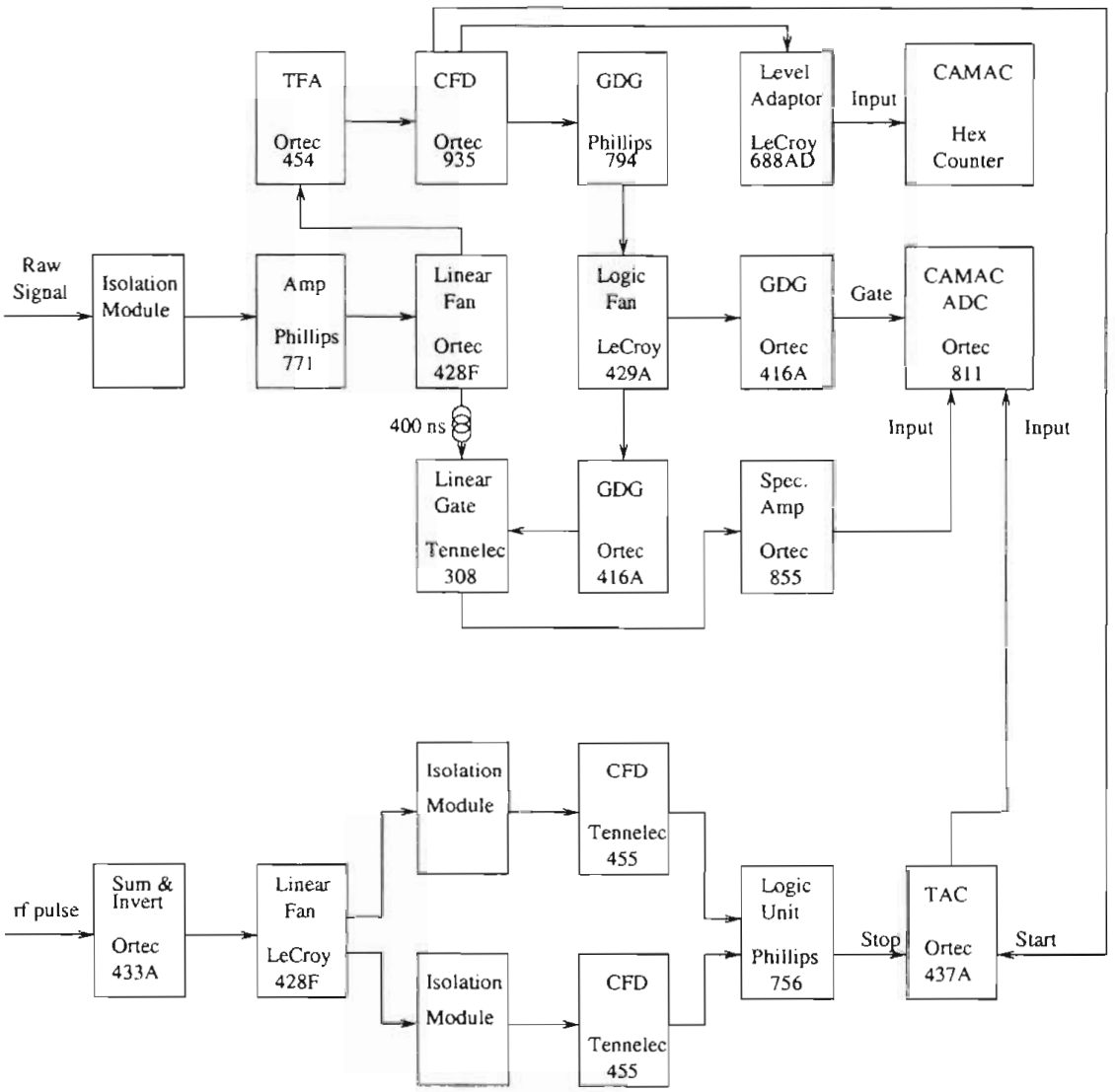

Figure 2.8: Electronics set-up for the off-axis NaI detector.

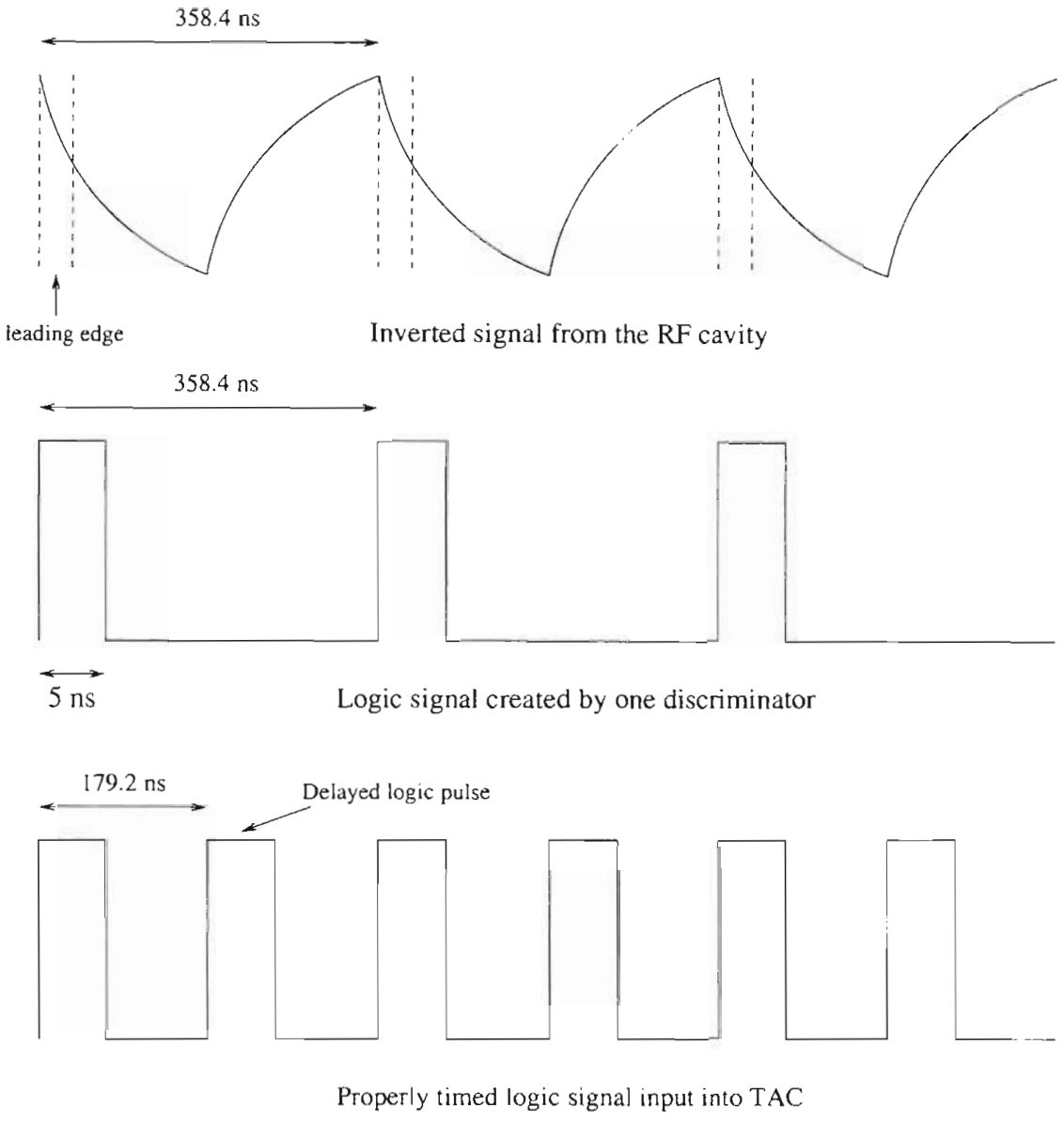

Figure 2.9: Schematic of the logic signal generated by the RF pulse. Figure not drawn to scale.

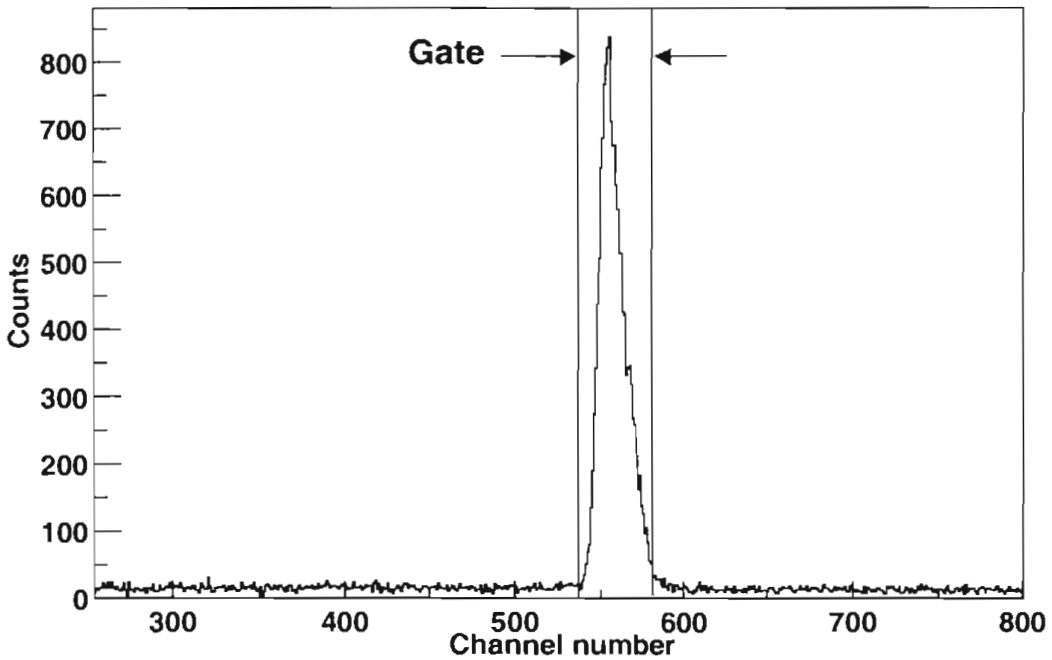

Figure 2.10: Typical TAC spectrum. A narrow gate was placed around the peak for the TAC-gated energy spectrum.

2.10. A software gate was placed around this peak to generate an energy spectrum of these events. An example of an energy spectrum with and without this software cut is shown in Figure 2.11. This figure clearly shows the reduction of two prominent background peaks, one at 2.6 MeV and another at 6.8 MeV.

2.5 Data Acquisition

The three main components of the data acquisition system, after the electronics, are the CAMAC modules, the MBD, and the VAX. The CAMAC modules are the modules which digitize the data, for example the ADCs and the counters. Once the ADC has digitized the signal, it generates a "look-at-me" (LAM) signal. This LAM signal tells the Multi-Branch Driver (MBD) that it has an event. It is the job of the

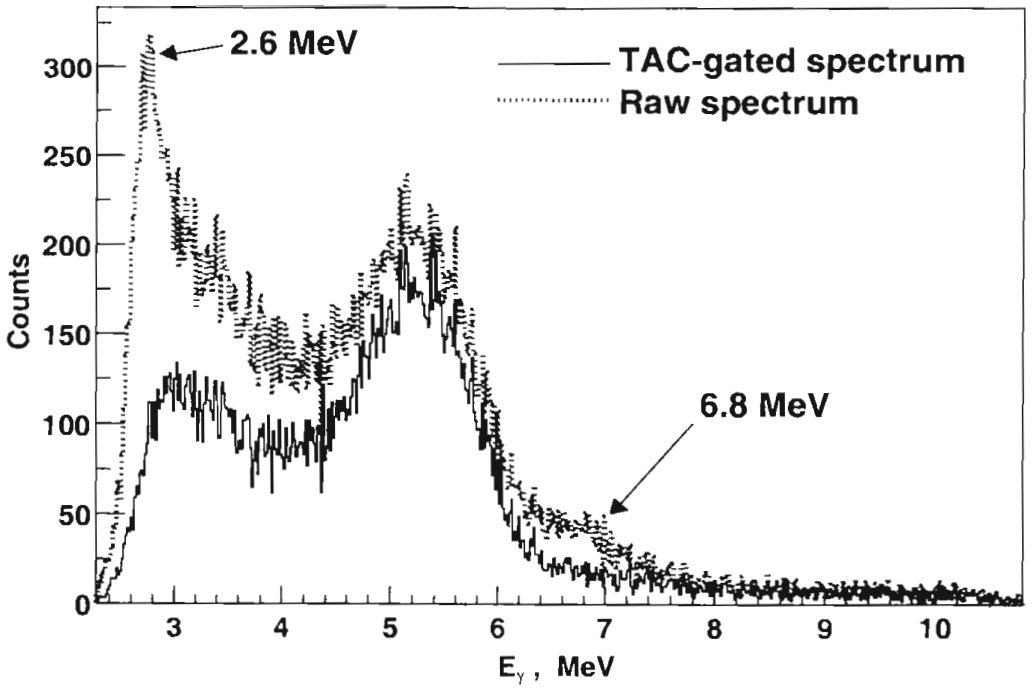

Figure 2.11: Spectrum for the off-axis NaI detector placed at 20° with 1/4" Cu scattering target and 15 MeV incident γ rays. The 2.6 MeV and 6.8 MeV peaks are standard background radiation lines, and these peaks are not as prominent in the TAC-gated spectrum. The sharp drop at the low-energy end represents the threshold set by the CFD, the peak at 2.6 MeV was partially cut out by this threshold.

MBD to send the event information to the VAX and enable the CAMAC modules to look for another event. The MBD then transmits the event information to the VAX. The VAX, based on an EVAL code, sorts the events into the different spectra. Once the proper spectra have been generated, they can be saved for offline analysis.

Chapter 3

Data Analysis

The main thrust of this work was measuring the γ-ray flux using an off-axis detector and an in-beam detector. Since a relative measure of the flux between both detectors is of primary importance, the data from both detectors were analyzed in a nearly identical manner.

3.1 Offline Analysis

An example of a raw spectra from the in-beam NaI is shown in Figure 3.1. The large peak is the γ-ray peak from the primary γ-ray beam. The low energy background is beam-related low energy radiation from various sources such as lead attenuators, the scattering target, and the collimator. The sharp cut-off of the low energy background represents the threshold set by the electronics.

In order to integrate the γ-ray peak and therefore extract a yield, the background is subtracted and the peak is fit to the response function of this particular NaI detector. This function was then integrated over the "one width up/two widths down" region. This was done using the analysis program ROOT which performs a χ^2 minimization technique using the MINUIT fitting procedure. To perform the most reliable fit to the raw data, the following procedure was performed. The background was fit to a function with an exponential form, then the response function was fit, and, finally, both functions were varied together until the χ^2 per degree of freedom was minimized. This procedure follows the same fitting procedure used by Laird Kramer and he provides a more detailed discussion which can be found in [Kra92]. The following sections briefly describe this fitting procedure.

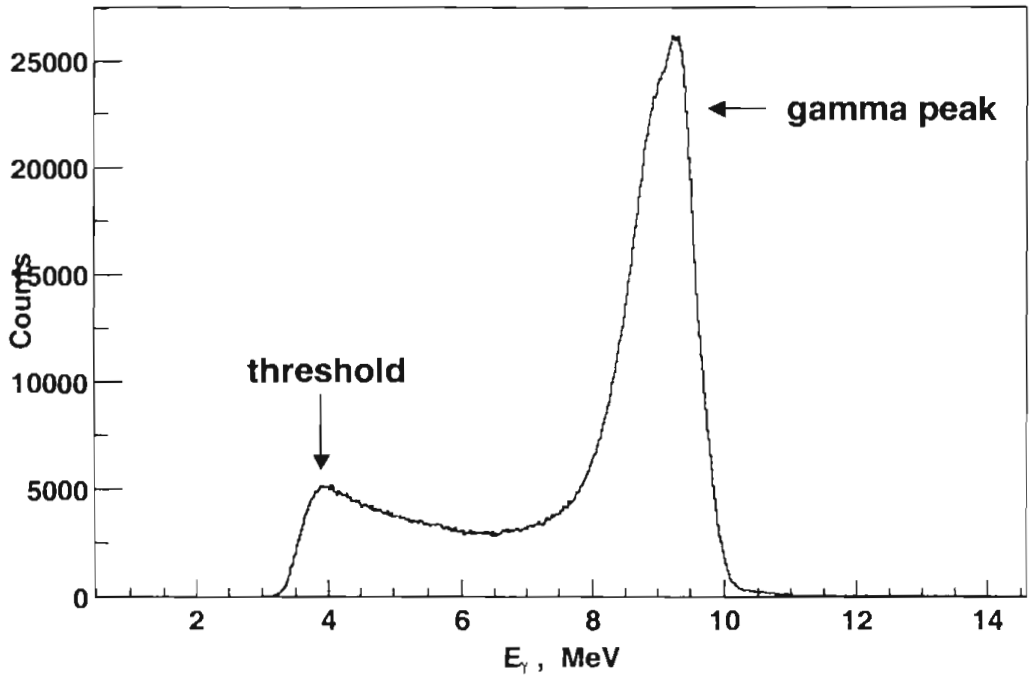

Figure 3.1: Typical in-beam NaI spectrum at 10 MeV with a 2" Pb attenuator in front of the detector face.

3.1.1 Background Subtraction

Though the γ-ray beam itself is very clean, its interaction with various materials placed in the beam, such as the collimator, produces additional background radiation. The sources of background for this experiment include the photoproduction of neutrons from the lead attenuators, natural room background, and scattering from the in-beam NaI, the collimator, and scattering target. From comparing background spectra which were taken when there was no γ-ray beam in the experimental area with spectra in which there was a γ-ray beam, it was evident that the dominant part of the background in both detectors was beam-related. For the in-beam NaI detector, the size and shape of the background was the same for nearly every run. For the off-axis NaI detector gated with the RF pulse, the shape of the background did not

vary much from run to run, it always had a shape which resembled an exponential decay (though this was not the case for the spectra which weren't gated with the RF pulse). The constancy of the shape of the background allowed it to be reliably fit to a function without knowing what actually comprised the background. From looking at "target-out" runs, it was also noticed that the scattering target itself introduced a fair amount of background radiation, which was another advantage to fitting the background as opposed to subtracting out the background from a "target-out" run.

The functional form used to fit the background was an exponential with a second-order polynomial argument:

$$b(x) = e^{A+Bx+Cx^2} \tag{3.1}$$

Other functional forms, such as a simple exponential or polynomial expansion, were tried, but the above function worked the best.

This function was then fit to the background based on two gates which were input parameters for ROOT. The lower gate was typically narrow and close to the low-energy threshold, or, put another way, as far from the γ-ray peak as possible. The upper gate was wider and started right after the leading edge of the γ-ray peak. Based on these two representative background gates, a χ^2 minimization was performed in order to determine the parameters A, B, C of $b(x)$.

3.1.2 Response Function Fit

In order to determine the functional form which best described the shape of the response function, the background was subtracted from a spectrum of the in-beam NaI in which the threshold was set very low and the detector was behind 2" of lead. This low threshold allowed much more of the low energy background to appear and therefore it could be fit very accurately. Normally it is a bad idea to take data with such a low threshold because the number of signals being digitized is greatly

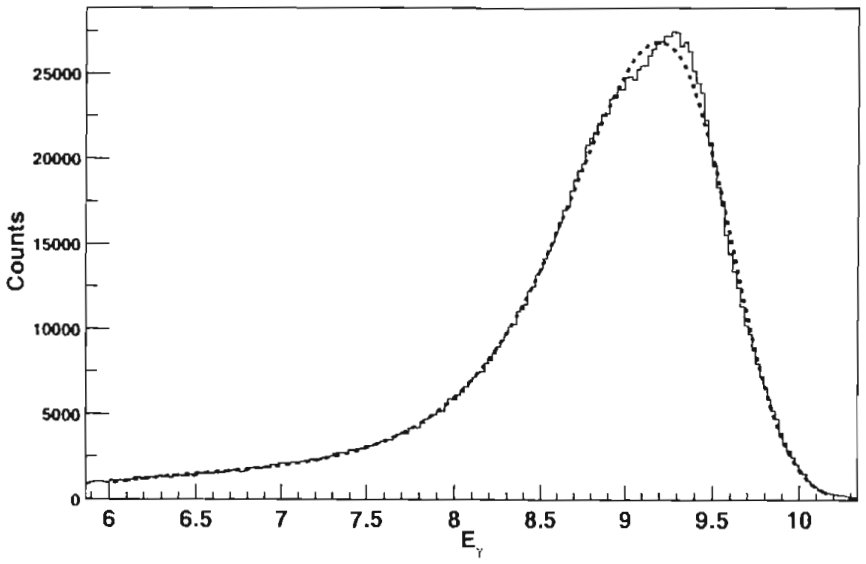

Figure 3.2: This plot shows the experimentally determined response function and the corresponding fit to that function. The functional fit (which is the dotted line) uses the parameters given in Table 3.1.

increased so that the dead-time correction becomes huge. Once the background was subtracted, this peak was then fit using two quartic exponential functions:

$$f(x) = e^{a+bx+cx^2+dx^3+ex^4} \quad (E_{low} \leq x \leq E_j) \tag{3.2}$$

$$g(x) = e^{f+gx+hx^2+ix^3+jx^4} \quad (E_j \leq x \leq E_{high}) \tag{3.3}$$

where E_j is where $f(x)$ and $g(x)$ are equal in magnitude and slope, and a-j are numerical coefficients. The eleven parameters were determined by performing a χ^2 minimization technique using the MINUIT fitting procedure. The values for the eleven parameters and the two cut-off energies are given in Table 3.1. Also a plot of the response function of the NaI detector as well as the functional fit to this response function are shown in Figure 3.2.

Since this same response function was to be used to fit the γ peak in all of the spectra for both detectors, it was necessary to transform the response function

Parameter	Value
a	-259.176
b	151.383
c	-32.0587
d	2.98665
e	-0.102678
f	453.782
g	-117.224
h	3.45209
i	1.12289
j	-0.0742192
E_j	9.26
E_{low}	5.0
E_{high}	10.3

Table 3.1: Parameters used in fitting the NaI response function for 10 MeV γ rays.

so that it would work for peaks of various sizes and at different energies. To do this, a geometric transformation was made to the variable of the function. The parameters of the transformation were determined by a χ^2 minimization. The three fitting parameters were the height, width, and centroid as defined below:

$$h(E) = He^{a+bE+cE^2+dE^3+eE^4} \quad (E_{low} \leq E \leq E_j) \tag{3.4}$$

$$i(E) = He^{f+gE+hE^2+iE^3+jE^4} \quad (E_j \leq E \leq E_{high}) \tag{3.5}$$

$$E = \frac{x - C}{W} + cent \tag{3.6}$$

where a-j are the original response function parameters in Table 3.1, *cent* is the measured centroid of the response function at 10 MeV, E is the energy of the channel, and H, C, and W are the three fitting parameters: height, centroid, and width, respectively. An example of the results of this fitting procedure on a spectrum from the off-axis NaI is shown in Figure 3.3.

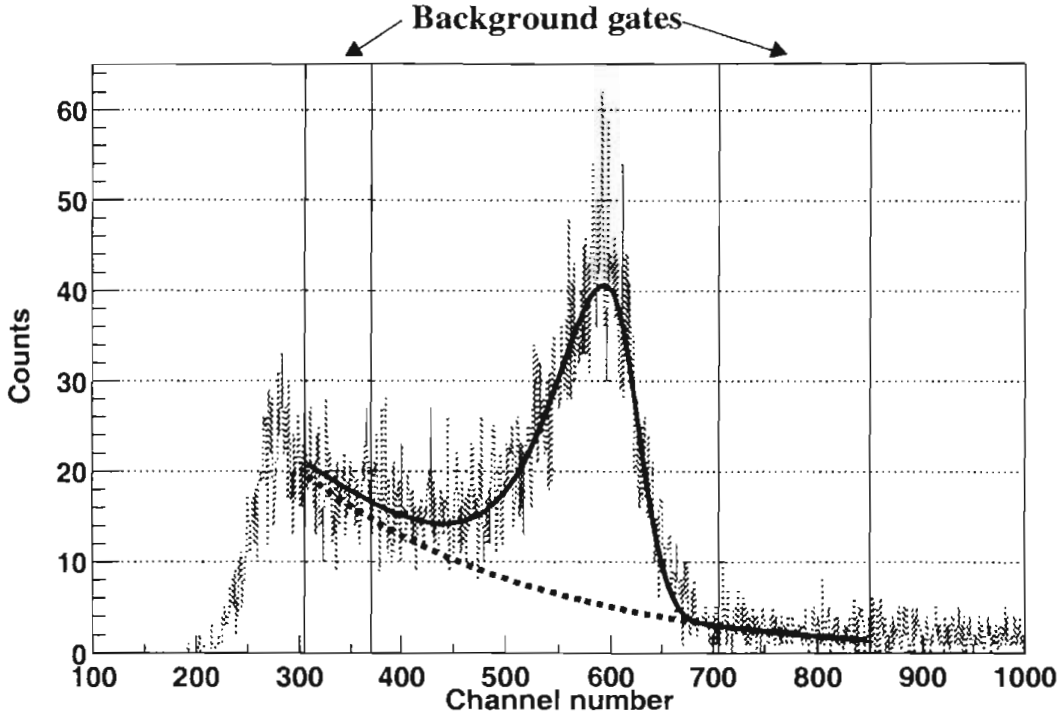

Figure 3.3: This figure shows a typical fit of the response function and the background to raw data. The dotted line is the background fit based on the two gates shown. The solid line is the response function fit superposed on the background fit. The data is from Compton scattering 10 MeV γ rays from a 1/4" Cu scatterer with the off-axis NaI placed at 10°.

3.1.3 Extraction of Yields

The input parameters for ROOT to perform the fitting procedure were the upper and lower bounds of each background gate, and calibration coefficients for a proper energy calibration of the spectra. Once these parameters were given, a rough fit to the background and the γ-ray peak was performed. Once a minimization was reached, the height, full-width at half-max, and centroid of the response function of the background-subtracted γ-ray peak was determined. Then the response function was integrated over the range determined by one full width above the centroid and two full widths below the centroid. The result of the integral was the yield used

to calculate the flux. The errors associated with this procedure will be discussed in Section 3.3.

3.2 Flux Calculation

Once the yields were extracted from the spectra, the flux could be calculated by making several corrections. The corrections made to both NaI detectors will be discussed in detail in the following sections.

3.2.1 In-Beam NaI Detector

The first step towards deducing a flux from the in-beam NaI was to extract a yield from the raw data. This was done using the procedure of subtracting the background, fitting the peak, and integrating over the region of interest which was just described. This yield was then divided by the data-taking time for that particular run to produce a raw count rate for the γ rays seen by the detector, and was then dead-time corrected. The next correction accounted for the detector efficiency. Since the yield only included counts in the region of interest, the raw count rate was just divided by the efficiency, ϵ, which was taken as 0.57 (as described earlier). Next the lead attenuation had to be taken into account. Unfortunately the attenuation of 2" of lead was not directly measured by putting it in and out of the beam at a low flux. Therefore, the attenuation was just calculated using the attenuation coefficients given by the National Institute for Standards and Technology (NIST) database [NIS]. The attenuation due to the 2" of lead used in this experiment was 94.4% at 10 MeV and 96.2% at 15 MeV. The same is true for the attenuation of the scattering targets, which was the next correction. The attenuation for the various scattering targets was given in Table 2.1. After all of these corrections, the results are the values for the fluxes given in the Results chapter. The errors involved in making these corrections are discussed

in Section 3.3.

3.2.2 Off-Axis NaI Detector

The first step in analyzing the data from the off-axis NaI was to extract a yield using the fitting procedure described in Section 3.1.3. This fitting procedure was performed on the spectra which were generated using the timing gate from the RF signal. The reason was because the spectra were cleaner and the background had a consistent shape and could, therefore, be reliably fit using Equation 3.1. The room background lines which showed up in the raw spectra, without the RF timing gate, complicated the background to the point where an exponential form was inaccurate.

Once a yield was extracted, the analysis proceeded in two directions. First, correction factors to an adjusted count rate in the off-axis detector were generated by comparing this count rate to the flux deduced from the in-beam NaI. The count rates in the off-axis NaI were adjusted by correcting for dead-time effects. This was done in an attempt to account for corrections which could not be easily reproduced in another experiment, and dead-time corrections are very specific to each experiment. The correction factors were then generated by dividing the flux deduced from the in-beam NaI by this adjusted count rate. These correction factors will be discussed in more detail in the next chapter.

The second phase of analysis was to deduce a flux from the yields extracted from the off-axis NaI data in a similar manner to the in-beam NaI, except with a few more corrections. From the extracted yield, a count rate was calculated and corrected for detector efficiency, dead-time correction, and the attenuation due to the 1 cm aluminum plate. The next step was to account for the Compton scattering in the scattering target. This meant determining the partial Compton scattering cross section subtended by the off-axis NaI detector from γ rays scattered from the target.

This was accomplished by multiplying the solid angle subtended by the detector by the differential scattering cross section which was given by the Klein-Nishina relation:

$$\frac{d\sigma}{d\Omega} = r_e^2 \Big[\frac{1}{1+\alpha(1-cos\theta)}\Big]^2 \Big\{cos^2\theta + \frac{\alpha^2(1-cos\theta)^2}{2[1+\alpha(1-cos\theta)]}\Big\}. \tag{3.7}$$

(This equation is the same as Equation 2.7 which was given in Chapter 2.) However, since the cross section varied over the face of the detector, the average value of Equation 3.7 over the angular range subtended by the detector was used,

$$\sigma_{partial} = (\Delta\Omega)\frac{1}{(\theta_2-\theta_1)}\int_{\theta_1}^{\theta_2}\frac{d\sigma}{d\Omega}d\theta, \tag{3.8}$$

with,

$$\Delta\Omega = \frac{A}{r^2}, \tag{3.9}$$

where A is the area which illuminates the back face of the NaI detector, r is the distance from the back face of the NaI detector to the scattering target, θ_1 and θ_2 correspond to the angular acceptance of the detector. Once the cross section was accounted for, the final step is including the effective target thickness (N) of the scatterer. Thus the flux calculation for the off-axis NaI can be summed up as:

$$Flux = \Big(\frac{Y}{\epsilon}\Big)\Big(\frac{dtc}{e^{-\mu_{Al}x}}\Big)\frac{1}{N}\Big(\frac{\Delta\Omega}{(\theta_2-\theta_1)}\int_{\theta_1}^{\theta_2}\frac{d\sigma}{d\Omega}d\theta\Big)^{-1}, \tag{3.10}$$

where Y is the raw count rate of the γ rays in the region of interest from the extracted yield, ϵ is the detector efficiency, dtc is the dead-time correction, $e^{-\mu_{Al}x}$ is the attenuation due to the aluminum plate, and N is the effective target thickness. The results of these flux calculations will be given in the Results chapter, as well as a comparison with the fluxes measured with the in-beam NaI.

3.3 Error Analysis

Most of the errror in this experiment was due to systematic uncertainty rather than statistical, especially when considering the in-beam NaI detector. And much of the systematic error could be reduced with a more careful attempt at this experiment in the future, especially in light of what has been learned by analyzing these data.

For the in-beam NaI, the error was almost purely systematic since the typical statistical error on the yield was 0.1%, which is negligible. The contributions to the systematic errors included the fitting procedure, lead attenuation, detector efficiency, and the target attenuation. The error on the background subtraction and the fit to the response function mainly had to do with the choice of the background gates. There was a certain amount of flexibility in choosing these gates, and, consequently, there were various results of the integrated yield for any given spectra. These different fits qualitatively looked adequate, while also giving similar values for the χ^2 minimization. To account for this uncertainty, the gates were varied until the fits were deemed unacceptable. The spread in the yields were taken as the extreme acceptable values and were then attributed as the error in the fitting procedure. The typical contribution for the in-beam NaI detector was 1%. It is worthwhile to note that the errors in this procedure were much larger in the analysis of the off-axis NaI due to poorer statistics, and could be reduced if a more thorough study were to be done in the future.

Determining the contribution of the lead attenuation to the total error was done by measuring the typical uncertainty on the thickness of the lead bricks used and the uncertainty in their position, and then calculating the effect of that uncertainty on the calculated attenuation. The error on the attenuation was determined to be 0.8%. This error could be reduced in the future with a direct measure of the attenuation. The error associated with the detector efficiency was 3%, which was a reasonable

Sources of Error for the In-Beam NaI Detector	
Source	Uncertainty
Extraction of Yield	1%
Dead-time Correction	1%
Detector Efficiency	3%
Pb attenuation	0.8%
Target attentuation	0.2%
Statistical	0.1%
Total	3.4%

Table 3.2: Uncertainties associated with the In-Beam NaI detector. For this table, the error attributed to the target attenuation was for a 1/4" Cu scattering target. All of the contributions were combined in quadrature to give the total error.

estimate based on previous measurements and simulations [Can01, Sab01]. The systematic uncertainty due to the target attenuation was very small since the actual target thicknesses were measured precisely and they were all thin enough so that multiple scattering was not an issue. By the same process as determining the error on the lead attenuation, the error associated with the target attenuation was 0.2%, though it varied according to the target. All of these systematic uncertainties along with the statistical uncertainty were combined in quadrature to give the total error. A summary of the uncertainties associated with the in-beam detector is given in Table 3.2.

The error associated with the off-axis NaI detector was much larger than the in-beam NaI, but, again, with a more careful experiment, the systematic uncertainties can be greatly reduced. As with the in-beam NaI, most of the error came from the systematic uncertainty, although the statistical uncertainty was larger for the off-axis detector which typically ranged from 1-2%. The sources of systematic uncertainty were the fitting procedure, the angle of the off-axis detector as well as the solid angle subtended, the attenuation of the aluminum plate, detector efficiency, target thickness, and the dead-time correction.

Sources of Error for the Off-Axis NaI Detector	
Source	Uncertainty
Extraction of Yield	2%
Detector Efficiency	3%
Dead-time Correction	1%
Al attenuation	1.3%
Target thickness	0.12%
Solid angle	0.76%
Angle	1.2%
Statistical	1%
Total	4.3%

Table 3.3: Uncertainties associated with the off-axis NaI detector. The errors shown are for the set-up where the off-axis detector was placed at 5° with a 1/4" Cu scattering target and 10 MeV incident γ rays. All of the errors were combined in quadrature to give the total error.

The background subtraction and fit to the response function was the biggest source of uncertainty. This was due to the fact that the count rate was much lower and therefore the peak to background ratio was much lower, thus making it harder to fit the peak. The uncertainty on the angle and solid angle subtended by the off-axis NaI was determined by considering the uncertainty on the measurements of both and then extrapolating the effect of that uncertainty on the partial cross section seen by the detector. This uncertainty was between 0.75-3.5%, depending on the experimental set-up at the time. The error due to the attenuation by the aluminum plate and the detector efficiency were calculated in the same manner as for the in-beam detector. The uncertainty in the actual target thickness was measured with a caliper. Since the scattering targets could be measured with high precision, the error associated with this uncertainty was below 1% for every target. All of the errors described above were combined in quadrature to give the total error. Because there were many different experimental set-ups, the contributions to the total error varied according to each set-up, however a summary of the errors for one experimental set-up for the off-axis

is shown in Table 3.3.

3.4 Monte Carlo Simulation

In addition to the primary experiment, some preliminary work was done by another member of the Radiative Capture group [Sab01] in attempting to simulate this experiment using GEANT, which is a Monte Carlo-based simulation program. In the future, more work will be done to fine-tune this simulation by including more accurate geometry and a more accurate description of the γ-ray beam.

3.4.1 GEANT

GEANT is a program which tracks the passage of particles through matter. The basic procedure in every simulation using GEANT is as follows:

- The geometry of the experiment is defined. This includes assigning a geometrical volume and material to every object in the experimental set-up, as well as making sure that they are properly positioned in relation to each other.

- The beam is established, which can be comprised of photons or charged particles. Many different properties for the beam can be input into the simulation, such as a finite width and energy distribution for the incoming beam.

- The beam is propagated using Monte Carlo generators. At every step along the path of a particle the probability of an interaction is calculated based on libraries of cross sections. Then an interaction may or may not happen based on the result of a Monte Carlo generator. The physics which are included are the electromagnetic interactions with matter (excluding neutrons), for example, the photoelectric effect, pair production, Compton scattering, Bremsstrahlung etc.

- The particles from the incident beam or which result from an interaction are tracked. For example, if a γ-ray is converted to an electron/positron pair in the scattering target, the trajectories of both the electron and positron are tracked and these particles are then free to interact with any matter in which they encounter. Finally, the energy deposition from particles (either photons, charged particles, or both) into an object specified by the programmer (in this case, NaI detectors) is recorded.

- Spectra can be generated which correspond to the energy deposited in the detector.

It is also possible to generate a 2-D image of the geometrical set-up and images of the various trajectories of photons or charged particles as the simulation is running. This is very useful as a consistency check when setting up the geometry of the experiment.

3.4.2 The Simulation

This simulation did a very good in considering the most important aspects of this experiment. Some of the more subtle aspects, such as γ-ray polarization, were not included, but will be included in future iterations of this simulation.

The γ-ray beam was simulated as a completely monochromatic beam of 10 MeV γ rays with a finite beam width of 2 cm. The width was created by defining a 1 cm circular region, and γ rays randomly passed through some part of this region based on a Monte Carlo generator. This simulation was run for 10^7 incident γ rays.

The geometrical set-up attempted to replicate the experimental set-up for 10 MeV γ rays incident on a 1/4" or 1/8" Cu scattering target with an in-beam NaI attenuated by 2" of lead and a collimated NaI detector placed at 5° with respect to the beam axis. The copper scattering targets were 2.5" square with a thickness of either 1/4" or 1/8". The NaI detectors were both 10" x 10" solid cylinders of NaI

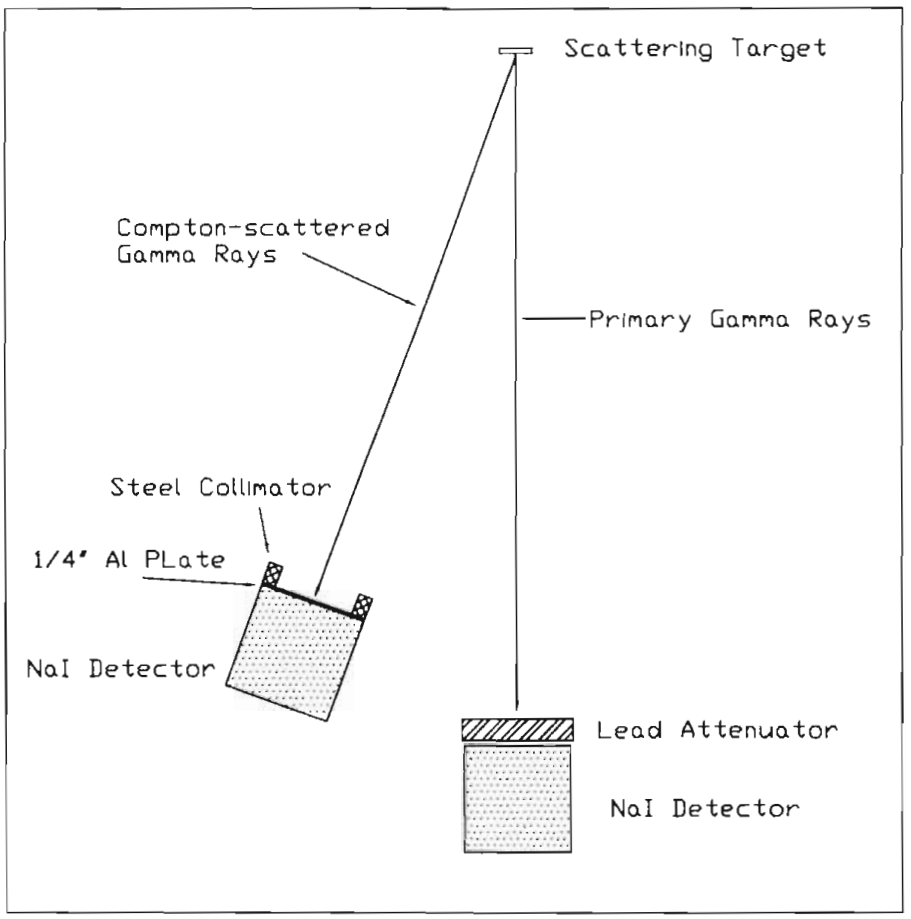

Figure 3.4: Geometrical set-up for the Monte Carlo simulation. Figure not drawn to scale.

crystal, with a thin aluminum casing surrounding them. The in-beam NaI had a lead wall directly in front of it which was 10.5" square and 2" thick. The off-axis NaI detector was oriented in such a way so that it was exactly 5° from the beam axis with its central axis pointing directly at the scattering target. Directly in front of this detector was a 1/4" thick, circular aluminum disc which completely covered the face of the detector. In front of that was a steel collimator which was simulated as a 2" thick steel cylinder with an inner diameter of 7.5" and an outer diameter of 10.5". And all of these objects were surrounded by air.

There were also many aspects of the experiment which were not included in this simulation, but will most likely be added in the future. Some of these exclusions include:

- The primary steel collimator as well as the plastic scintillating paddle.
- The polarization of the incident γ rays.
- A 2" lead wall which shielded the off-axis NaI from the in-beam NaI.
- A lead wall which shielded the off-axis NaI from the primary collimator.
- The beam dump, which includes the Pb-glass detector as well as the shielding surrounding the Pb-glass detector.
- The earth's magnetic field.

Even without the exclusions just discussed, the results of this simulation are reasonably close to the results of the experiment. Which is yet another reason why this technique is showing a lot of promise as a possible beam-intensity monitor.

Chapter 4

Results

Correction factors to the count rates in the off-axis detector which convert these results to actual γ-ray fluxes were determined. In addition, a more thorough study of the off-axis NaI detector was done at 10 MeV and actual γ-ray beam fluxes were deduced from the raw count rate and were compared with the fluxes determined from the in-beam NaI. Finally, some preliminary measurements were done with the plastic scintillator and Pb-glass detector, which are currently being used as rough beam monitors.

4.1 Flux Calculation Results

By applying the corrections to the raw count rates discussed in Section 3.2 to both NaI detectors, the incident flux was deduced from both of these count rates and then compared to each other to see how well they agreed with one another. At 10 MeV, the yields were determined by subtracting the background and integrating the fit to the response function over the region of interest. These yields were dead-time corrected and then used to calculate the flux. Fot the in-beam NaI, this meant correcting for the lead attenuator, target attenuation, and detector efficiency. For the off-axis NaI, this meant correcting for the aluminum plate attenuation, detector efficiency, effective target thickness, and partial cross section. Figure 4.1 shows the results of the calculated fluxes for different types of scattering targets and several angles.

The fluxes given in Figure 4.1 have been averaged over different runs for a given target and angle, and runs in which the peak could not be adequately fit to the response function due to poor statistics in the off-axis detector have not been included.

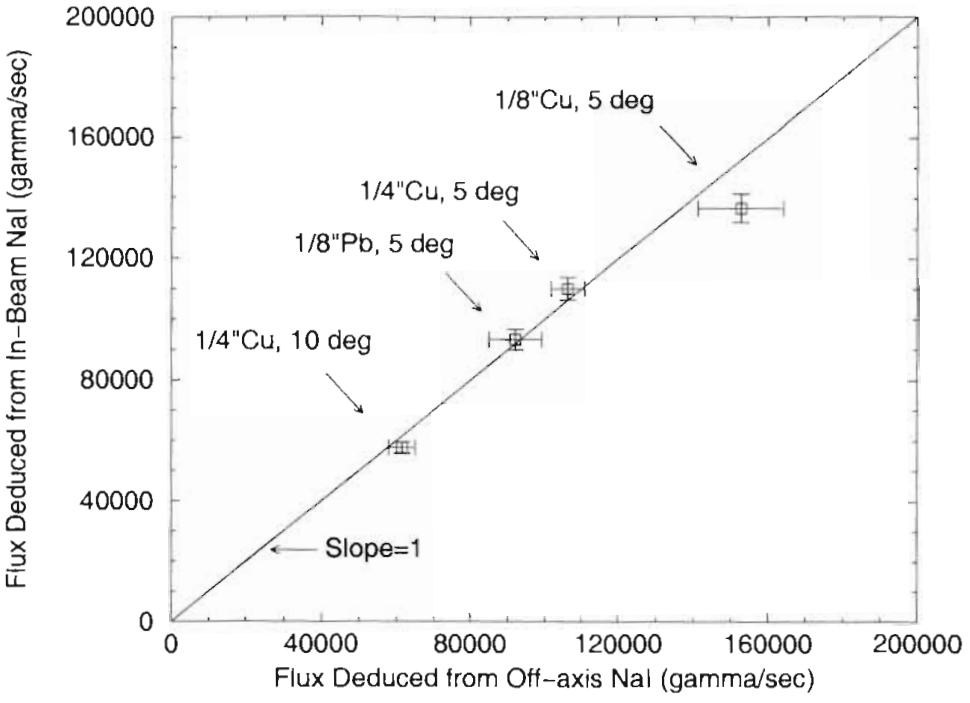

Figure 4.1: Flux deduced from the in-beam NaI versus the flux deduced from the off-axis NaI. The straight line plotted in the center has a slope of 1. The error bars include statistical and systematic uncertainties.

The error bars associated with the flux deduced by the in-beam NaI ranged from 3.4-3.5%, while the errors for the off-axis NaI range from 4.3-7.7%. Data that were not shown are from runs in which the dead-time correction was greater than 30% or where the error due to the peak fitting was greater than 12%. Also the data at 15 MeV were not fully analyzed and are therefore not included, however the correction factors given in the next section suggest that the 15 MeV data will give similar results.

4.2 Correction Factors

At fluxes between 10^4-10^6 γ/sec, the method of measuring the fluxes with an in-beam NaI is reliable to within a few percent. But for use in future experiments, it is undesirable to place a NaI detector and lead attenuators in the beam since

they can cause a lot of background radiation which may interfere with the primary experiment. Therefore, so that these results will be immediately useful as a beam-intensity monitor, empirical correction factors were calculated for the off-axis NaI count rate. These correction factors can be used by replicating any of the various set-ups in this experiment without a NaI detector in the beam. In the future, a more detailed and improved study should be performed at different energies and incident fluxes. Possible improvements to this experiment will be discussed in Section 5.2.

Table 4.2 is the result of all of the acceptable data taken. Some of the data had very poor statistics due to contraints on the data-taking time, and, as a result, the correction factors have large error bars. As discussed in Section 3.3, the dominant contribution to the error on these runs with poor statistics is the fitting procedure. The Correction Factor Tables were generated in the following manner:

- The in-beam NaI count rates shown were calculated from the background-subtracted yield in the region of interest.
- The fluxes deduced from the in-beam NaI count rates were calculated using the corrections given in Table 4.1.

In-Beam NaI	Off-Axis NaI
Detector efficiency	Detector efficiency
Lead attenuation	Aluminum plate attenuation
Target attenuation	Dead-time correction
Dead-time Correction	

Table 4.1: Corrections made to the count rates in both NaI detectors in generating the correction factors.

- The off-axis count rates were determined from the yields extracted from the spectra which were gated with the RF signal. They were then corrected according to the corrections given in Table 4.1.

- The Correction Factors (C.F.) were calculated by simply dividing the flux deduced from the in-beam NaI by the count rate in the off-axis NaI, with the corrections just discussed.

- The error associated with the correction factors are the propagation of the errors on the deduced flux and the count rate, which were determined according to the discussion in Section 3.3.

- The naive prediction is a prediction of how the correction factors for various experimental set-ups should be related to each other. For example, for a given incident flux, the count rate in the off-axis NaI with a 1/8" Cu target would be expected to be roughly half of the count rate with a 1/4" Cu target, therefore, the correction factor for the 1/8" Cu target should be twice that of the 1/4" Cu target. The predictions given actually show how the *inverse* of the correction factors relate to one another, since it is intuitively easier to understand.

- The actual relationships of the inverse of the correction factors were calculated and are given in the last columns in Table 4.2.

4.3 Simulation Results

Once the simulation is complete, the energy which has been deposited in each detector can be presented in the form of a spectrum similar to the energy spectra in the actual experiment.

Correction factors can be generated in a similar manner as in Section 4.2. A yield was extracted from the spectra from the simulation by simply integrating the peak over the "one width up/two widths down" region of interest. Since this was just a preliminary analysis, no attempt to subtract the background was made. This yield was then corrected for the aluminum plate attenuation and the detector efficiency,

10 MeV Incident γ rays at 5°

Target	0° flux (10^5 γ/s)	Off-axis c.r. (counts/s)	C.F.	Error (%)	Naive Prediction	Actual
1/8" Cu	1.37	25.4	5391	8.3	0.5	0.64
1/4" Cu	1.10	32.1	3428	5.5	1	1
1/8" Pb	0.93	20.2	4617	8.4	0.66	0.74

10 MeV Incident γ rays and a 1/4" Cu Scatterer

Angle	0° flux (10^5 γ/s)	Off-axis c.r. (counts/s)	C.F.	Error (%)	Naive Prediction	Actual
5°	1.10	32.1	3428	5.5	1	1
10°	0.57	13.7	4213	6.7	0.72	0.81
20°	1.71	17.7	9658	15.8	0.27	0.35

15 MeV Incident γ rays and a 1/8" Cu Scatterer

Angle	0° flux (10^6 γ/s)	Off-axis c.r. (counts/s)	C.F.	Error (%)	Naive Prediction	Actual
5°	0.86	100.4	8595	10.0	2.52	3.55
10°	0.92	52.0	17767	6.3	1.6	1.72
15°	1.14	37.5	30515	5.7	1	1

15 MeV Incident γ rays and a 1/4" Cu Scatterer

Angle	0° flux (10^6 γ/s)	Off-axis c.r. (counts/s)	C.F.	Error (%)	Naive Prediction	Actual
5°	2.42	487.2	4967	7.2	1.57	1.81
10°	1.54	166.0	9300	6.3	1	1
15°	3.38	255.0	13262	10.2	0.62	0.70
20°	2.05	99.3	20683	8.6	0.38	0.44

Table 4.2: Correction factors for scattering 10 and 15 MeV γ rays from various scatterers and detected at various scattering angles. The naive predictions for the first table are based on the differing target thicknesses of the various scattering targets. The naive predictions in the next three tables are based on the differing values of the partial scattering cross section (Equation 3.8) at the various scattering angles.

Simulation of 10 MeV Incident γ rays at 5°							
Target	0° flux (10^7 γ/s)	Off-axis c.r. (counts/s)	C.F. (sim.)	Naive Prediction	Actual (sim.)	C.F. (exp.)	Actual (exp.)
1/8" Cu	1	1058	5200	0.5	0.57	5391	0.64
1/4" Cu	1	1864	2951	1	1	3428	1

Table 4.3: Correction factors from simulating 10 MeV γ rays scattered from various scattering targets and detected at 5°. The naive predictions are based on the differing target thicknesses of the various scattering targets.

which was taken as 57.3%. This efficiency is based on the results of another simulation which simulated the in-beam NaI. The spectrum generated by this simulated NaI was integrated over the region of interest and then divided by the total number of counts, and an efficiency of 57.3% was obtained [Sab01]. To generate the correction factor, the total number of incident γ rays was divided by this yield. These correction factors are given in Table 4.3, which are organized in the same manner as the correction factor tables given in Section 4.2. The last two columns are the correction factors and the actual relationship between the inverse of the correction factors which were determined experimentally.

4.4 Preliminary Measurements

The results of the preliminary studies done on the plastic scintillator and the Pb-glass detector give empirical values for the efficiency of each detector at 10 MeV. These measurements serve as a starting point for future studies aimed at cross-calibrating all of the detectors which will serve as beam monitors.

4.4.1 Plastic Scintillator

At DFELL, a plastic scintillator is being used as a beam monitor to let both the experimenter and the FEL operator know that γ rays are passing through the collimator

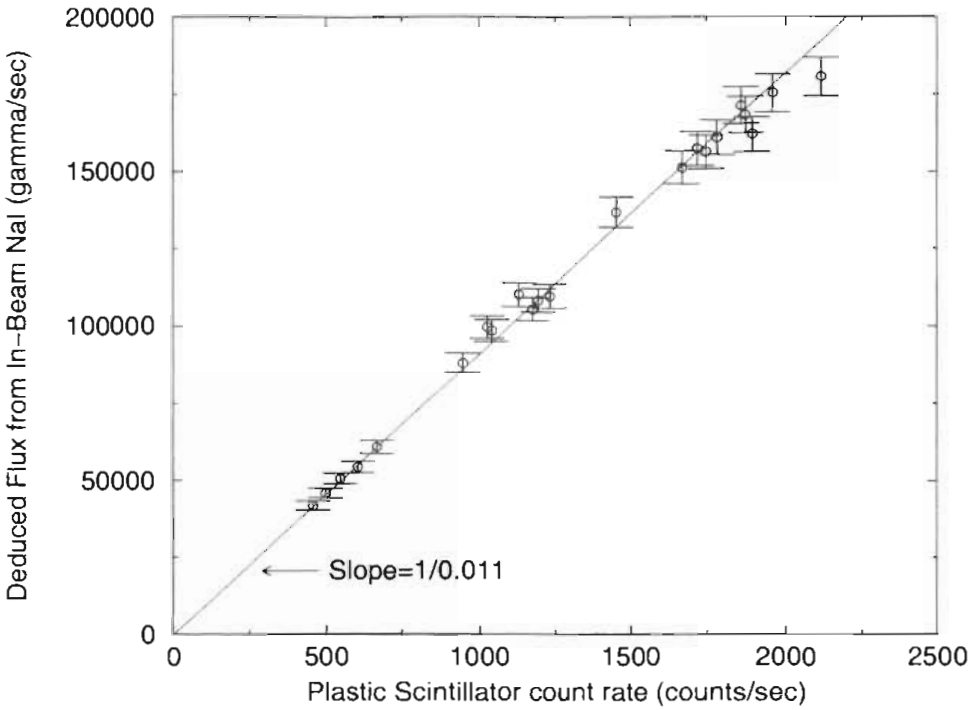

Figure 4.2: Flux deduced by the in-beam NaI versus the count rate in the plastic scintillator. The above data is for 10 MeV incident γ rays and no scattering target. The slope of the line is the inverse of the calculated empirical efficiency. No error bars have been placed on the plastic scintillator's count rate.

while also giving them a rough idea of the flux. It is primarily used for tuning the γ-ray beam. Therefore it is useful to get a better idea of the efficiency of this plastic scintillating paddle. Figure 4.2 is a plot of the deduced flux seen by the in-beam NaI as a function of the average count rate in the plastic scintillator for that given flux, all of these data points are with 10 MeV incident γ rays and no scattering target in place. By simply dividing the count rate in the plastic scintillator by the calculated flux, an approximate value for the efficiency of the plastic scintillator is found. The result of this calculation gave an efficiency for the paddle of $1.10\% \pm 0.04\%$, where the uncertainty is just the statistical uncertainty of the set of data points. It is important to note that this efficiency is a rough approximation, and that the uncertainty

does not include systematic uncertainty and is therefore unrealistically small. The biggest source of systematic uncertainty is the contribution of charged particles to the plastic scintillator's count rate. Since it was placed directly after the primary collimator and no attempt was made to deflect charged particles produced by the collimator, possibly a significant portion of the counts in the plastic scintillator are charged particles. This contribution could not be reliably estimated and therefore no attempt was made to make more reasonable error bars. Despite these uncertainties, in the future, this efficiency can be used as an empirical result for this particular experimental set-up.

4.4.2 Pb-Glass Detector

An attempt was made to correlate the Pb-glass detector with the fluxes deduced by the in-beam NaI. Since a direct flux measurement means that the NaI detector is placed in the γ-ray beam, the Pb-glass detector could not detect γ rays at the same time. Therefore in order to correlate the Pb-glass detector with the in-beam NaI, it was first correlated with the plastic scintillator, and then cross-correlated to the in-beam NaI by correcting the count rate in the plastic scintillator using the efficiency determined in the previous section. Figure 4.3 shows the results of this cross correlation.

The circular data points correspond to runs in which there was no scattering target in place. The square data points correspond to runs in which there was a scattering target and these points have been corrected by the total attenuation due to the target. Calculating the efficiency in the same manner as the paddle gives an efficiency of 28.5%$\pm$0.2%. Again, the uncertainty is statistical only, and this result should only be used as an empirical result since it was calculated from another empirical result. This result for the efficiency will be discussed in more detail in the

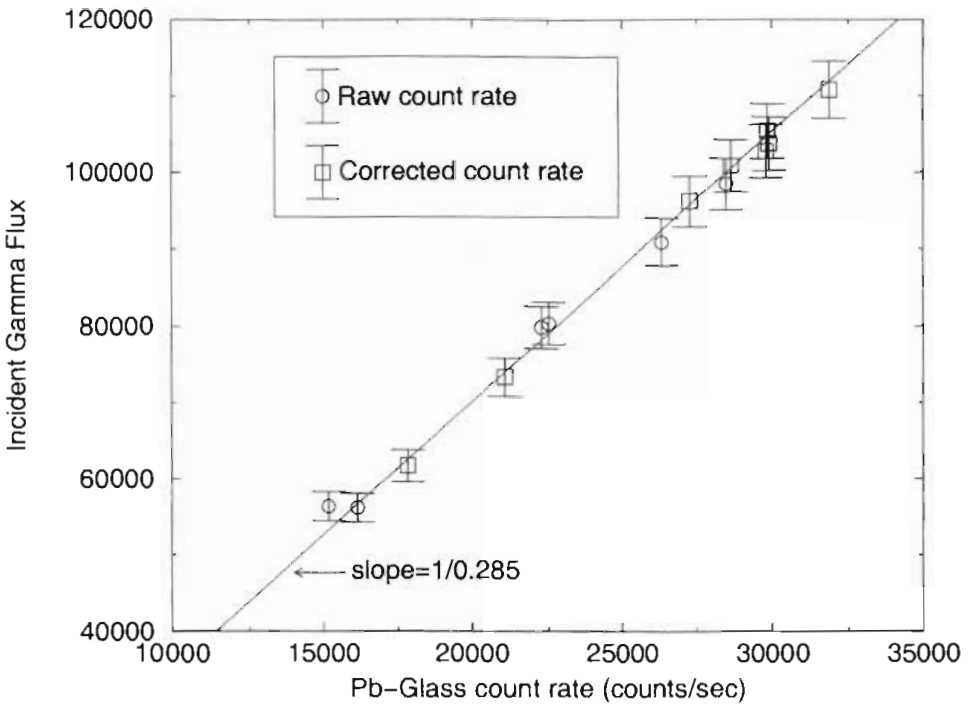

Figure 4.3: Incident γ-ray flux versus the count rate in the Pb-glass detector. The incident γ-ray flux was determined from the paddle count rate which was corrected using an efficiency of 1.10%. The corrected count rate has been corrected for the scattering target attenuation, while the raw count rate had no scattering target in place. The above data is for 10 MeV incident γ rays.

Summary chapter.

Chapter 5

Summary

A direct measurement of the γ-ray flux at 10 and 15 MeV was done with an uncertainty of 3-4%. At the same time, a new technique to measure the γ-ray fluxes indirectly by detecting the Compton-scattered γ rays from a thin scatterer at a particular scattering angle was also performed. Correction factors to the count rates in the off-axis detector which convert these results to the actual γ-ray flux rates were determined for several scattering targets and several angles at both 10 and 15 MeV. In addition, the total incident γ-ray fluxes were calculated from the count rates in the off-axis NaI detector and were found to agree with the direct measurements to within a 5% uncertainty. Preliminary measurements on a plastic scintillator and Pb-glass detector were performed and empirical values for their efficiencies were determined for immediate use by experimenters currently working on experiments at HIGS.

5.1 Discussion of Results

The results from the comparison of the fluxes deduced from the in-beam NaI and the off-axis NaI demonstrate that this technique has a lot of promise as a beam-intensity monitor. From the results of the comparison of the deduced fluxes and the correction factors, some general conclusions can be made.

Both copper and lead were adequate as target materials, however copper has characteristics which make it a better scatterer at energies of 10 and 15 MeV. The electron number density is only slightly less than that of lead, while the total attenuation of the γ-ray beam is much less for copper. Also the cross section for the photoproduction of neutrons from copper is much less than for lead, at all energies.

These advantages make copper better since it can provide similar count rates without introducing as significant a background contribution as a lead target of the same thickness. Another advantage for copper over lead deals with the determination of the actual target thickness. Since lead is a very soft metal, everyday handling of the targets causes them to become deformed. As a result the measurements of the actual target thicknesses have greater uncertainty than for copper. There are also other alternative materials to copper which have not been explored and may be better suited as a scatterer, for example nickel is a very promising candidate.

The results of this thesis do not point to an ideal effective target thickness (e/cm^2) of the scatterer for a given flux. But they do provide support for an upper limit to this thickness. Since the results for the 1/4" copper target came out very well for fluxes which are at the lower end of the range of fluxes for the γ-ray beam at HIGS ($10^5\gamma$/sec), there is no need to try targets with an effective target thickness greater than 1.56×10^{24} e/cm^2, which is the target thickness for a 1/4" Cu target. With HIGS routinely providing γ-ray fluxes of greater than 10^6 γ/sec at energies as low as 5 MeV, a 1/8" copper scattering target should be adequate for providing a decent count rate in the off-axis NaI while not introducing a significant amount of background radiation.

When analyzing the data, it was noticed that the error due to the background subtraction was generally less at an angle of 10° compared to all other measured angles, at both 10 and 15 MeV. At 5°, the background-to-peak ratio was greater, which suggests that there was forward-peaked beam-related background radiation, possibly from the collimator, scattering target, the in-beam NaI, the beam dump, or some combination. The collimator and the scattering target are the most obvious choices for producing beam-related background in the off-axis NaI since the off-axis NaI was well-shielded from the in-beam NaI and beam dump. The off-axis NaI was still shielded from the primary collimator, but, since the background from the colli-

mator is expected to be large, it may be possible that the shielding was inadequate. At larger angles (15-20°) the threshold was set too close to the Compton-scattered γ-ray peak which complicated the background subtraction (the threshold was set to cut out a significant peak from room background radiation). This could have been improved by simply lowering the threshold since the RF gate cut out most of this background radiation anyway. In the future, though, it is a good practice to try to keep the energy of the Compton-scattered γ rays different from any natural room-background γ-ray peaks by choosing the scattering angle appropriately. Even though the RF timing reduced most of this background, the best solution is to avoid it altogether, when possible.

The correction factors generated in this thesis will be of immediate use for experiments which are planned to happen very soon in the HIGS program. These factors rely on the accuracy of the direct measurement of the γ-ray flux with an in-beam NaI. The correction factors with an uncertainty near 5% will be the most useful since no absolute cross section measurements requiring greater accuracy are planned for the immediate future. Knowing the flux to an accuracy of 5% is more than adequate for asymmetry measurements. The correction factors with a greater uncertainty ($\sim$10%) will probably not be useful since they are mainly a result of poorer statistics due to either a target being too thin or an angle being too large.

The results of the Monte Carlo simulation agree reasonably well with the experimentally determined correction factors. There was some discrepancy between the simulation and experiment, however, and this is most likely due to simplifications we made in the simulation, such as leaving out some shielding walls and neutron background. Qualitatively, the difference between the naive prediction and the actual relationship of the correction factors in doubling the target thickness was verified in the simulation. Hopefully this simulation will be useful in understanding many

aspects of the experiment - specifically the effects of the attenuation of γ rays in the scattering target after they have been Compton scattered. This effect was not taken into account in the analysis of the data from the off-axis NaI.

The preliminary studies done on the plastic scintillating paddle and the Pb-glass detector were useful in determining empirical efficiencies. With recent modifications to the collimator set-up in the experimental area, new measurements on the plastic scintillator should be done to see if similar results are obtained. Future experiments to study the plastic scintillator could involve mapping out the efficiency for different γ-ray energies.

Further studies also need to be done on the Pb-glass detector. The empirical efficiency of 28.5% is lower than expected, and this was probably due to missed γ rays which were below the threshold set for the detector. Since the energy resolution is so bad it was difficult to know where the threshold was set. Previous studies [Vog95] have shown that the energy resolution for 20 MeV photons is $\sim$90%, and is expected to worsen rapidly with decreasing incident photon energy. With this type of energy resolution it is difficult to extract any reliable conclusions from the present work. Also discussed in the paper by Vogt was the fact that these detectors have a "natural threshold of several MeV." Without a better knowledge of how these detectors perform at energies between 5-50 MeV, this Pb-glass detector cannot serve as a reliable beam monitor.

5.2 Future Improvements

Many improvements can be made to this technique which will most likely reduce the statistical and systematic error on both detectors. Those improvements include additional measurements, better ideas for shielding, and a more thorough use of Monte Carlo simulations.

The first suggestions have to do with performing additional measurements to reduce some of the systematic uncertainties. One of these would be the direct measurement of the efficiency of both NaI detectors. While another would be the determination of the "true" response function of each detector, since the response functions used in this experiment were determined from a peak which needed to have a significant background contribution subtracted off. By placing a NaI detector with no lead attenuator in the γ-ray beam at very low fluxes and taking special care to sweep any charged particles away, both of these measurements can be performed. By lowering the threshold, a true response function with virtually no background contribution is obtained. The response function can then be fit with a greater accuracy. This function can be integrated to obtain the actual detector efficiency, thereby reducing this contribution to the total systematic uncertainty for both detectors. In this work, this uncertainty in the detector efficiency had an unfortunately large contribution of 3%.

Another measurement which could be performed at low flux would be to carefully measure the attenuation of specific lead attenuators of several different thicknesses. These lead attenuators can then be marked and set aside for future use. The same process could also be done to characterize the attenuation of a set of scattering targets.

Another way to lower the systematic uncertainties would be to perform a more focused experiment. Many different angles and scattering targets were used for this experiment, and, as a result, the statistical uncertainty in the off-axis detector was large, which also contributed to a systematic uncertainty in trying to fit the peak. Future experiments would only need one set-up and could obtain much better statistics, and it would allow for a very precise measure of the angle and solid angle of the off-axis NaI detector.

There are also improvements which can be made to the shielding of both NaI detectors. The first suggestion would be to place a sweep magnet after the primary collimator and the scattering target to sweep away charged particles. Another improvement, which has already been discussed numerous times in this thesis, would be to replace the 1cm aluminum plate with a veto paddle. In addition, another veto paddle could be placed in front of the in-beam NaI, which would veto a lot of the charged particles which stream out of the lead attenuators. It was also noticed that placing the lead attenuator far away from the in-beam NaI reduced the amount of background radiation incident on the detector. "Far away" means as far as possible without introducing background into other detectors involved in the experiment, specifically the off-axis NaI detector.

One last suggestion would be to generate correction factors which will be more useful in a variety of situations. These correction factors are empirical and therefore require a nearly exact replication of the experimental set-ups which produced them. Therefore, they will only be reliable (to the uncertainty claimed in this thesis) at the same γ-ray energies. The reason this is true is because many factors change when the incident γ-ray energy changes, such as the attenuation of various materials, and the neutron background contribution. Therefore it would be useful to perform an experiment to generate these correction factors with one scattering target and scattering angle, but with many different incident γ-ray energies.

5.3 In Closing

With the current γ-ray fluxes of greater than 10^6 γ/sec through the primary collimator at γ-ray energies ranging from 5-60 MeV, the HIGS program is now in a position to perform unique and thorough experiments in nuclear physics in a reasonably short amount of time. With planned upgrades, the flux is expected to increase to 10^9 γ/sec

which will make experiments once thought impossible to be suddenly very feasible. Therefore the need for a flux monitor is of immediate importance to this facility, and, hopefully, the work done in this thesis in developing this new technique will be the first stepping stone to having a γ-ray beam-intensity monitor which can measure γ-ray fluxes to an accuracy of 1% or better, even at fluxes as high as 10^9 γ/sec. Thank you and good night.

Appendix A

Set-up Parameters

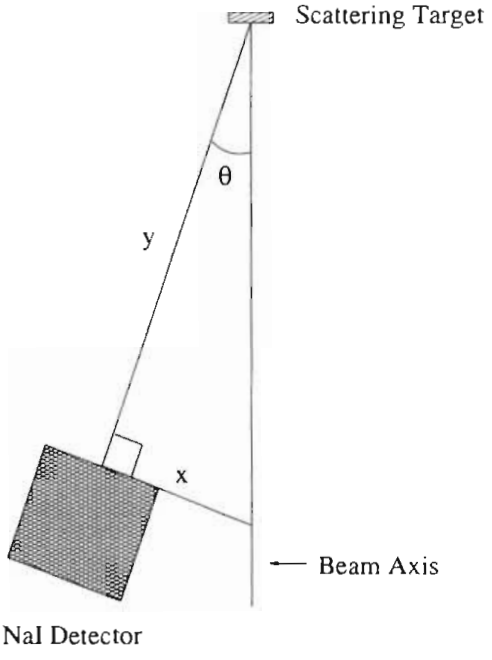

Figure A.1: Schematic of measurements used to determine the angle of the off-axis NaI detector.

Figure A.1 illustrates what dimensions were actually measured in determining the angle of the off-axis detector. To make these measurements a "T" can be used to angle the off-axis NaI so that it points towards the scattering target and then the perpendicular (x) can be measured from the center of the NaI face to the beam axis by using an alignment laser. The following tables give the measured values of x and y for every angle used in this experiment, as well as the actual values for θ determined from these measurements.

The actual target thicknesses and the calculated effective target thicknesses are

Angles Used at 10 MeV

Angle	x $\pm$ σ_x	y $\pm$ σ_y	Actual Angle
5°	10.875" $\pm$ 0.125"	123.5" $\pm$ 0.5"	5.03° $\pm$ 0.06°
10°	21.0" $\pm$ 0.5"	123.25" $\pm$ 0.5"	9.67° $\pm$ 0.24°
15°	32.0" $\pm$ 0.5"	123.25" $\pm$ 0.5"	14.55° $\pm$ 0.24°
20°	48.0" $\pm$ 0.125"	123.25" $\pm$ 0.5"	21.28° $\pm$ 0.11°

Table A.1: Actual angles used for the 10 MeV experiments.

Angles Used at 15 MeV

Angle	x $\pm$ σ_x	y $\pm$ σ_y	Actual Angle
5°	10.5" $\pm$ 0.125"	121.5" $\pm$ 0.5"	4.94° $\pm$ 0.06°
10°	21.0" $\pm$ 0.75"	120.0" $\pm$ 0.5"	9.92° $\pm$ 0.36°
15°	31.0" $\pm$ 0.75"	120.0" $\pm$ 0.5"	14.50° $\pm$ 0.36°
20°	43.25" $\pm$ 0.25"	120.0" $\pm$ 0.5"	19.82° $\pm$ 0.15°

Table A.2: Actual angles used for the 15 MeV experiments.

given in Table A.3. All of the targets were measured several times with a high precision caliper. The errors on the measured thicknesses are the standard error on the mean. No error was associated with the density. Also given in this table are the calculated effective target thicknesses.

Parameters for the actual scattering targets

Target	Measured thickness [inches]	Density [g/cm^3]	Effective Target Thickness [10^{24} e/cm^2]
1/4" Cu	0.2471" $\pm$ 0.0003"	8.96	1.5458
1/8" Cu	0.1233" $\pm$ 0.0003"	8.96	0.7714
1/8" Pb	0.1483" $\pm$ 0.0009"	11.34	1.0186

Table A.3: Actual target thicknesses used for this experiment.

Appendix B

Relevant Information for Possible Scattering Targets

Some of the targets listed in Table B.1 would make very good scattering targets, while others would make horrible scattering targets, while still others would make very impractical targets because they would be obscenely expensive. Nevertheless, the relevant properties of many materials which could be considered for a scattering target are given below.

Relevant information for possible scattering targets

Material	Z	A	ρ [g/cm^3]	N [$10^{24}\frac{e}{cm^3}$]	μ_{tot}/ρ [$10^{-2}\frac{cm^2}{g}$]	$\sigma_{\gamma n}$ [mb]
Titanium	22	47.90	4.54	1.257	2.73	0
Iron	26	55.85	7.86	2.204	2.99	0
Nickel	28	58.71	8.902	2.557	3.18	0
Copper	29	63.54	8.96	2.463	3.10	0
Zinc	30	65.37	7.133	1.972	3.18	0
Gallium	31	69.72	5.904	1.860	3.13	0
Molybdenum	42	95.95	10.22	2.695	3.65	~25
Palladium	46	106.4	12.02	3.131	3.80	~30
Silver	47	107.9	10.5	2.756	3.88	~25
Cadmium	48	112.4	8.65	2.225	3.85	~30
Tin	50	118.69	7.31	1.855	3.90	~30
Tantalum	73	180.95	16.654	4.047	4.72	~90
Tungsten	74	183.85	19.3	4.860	4.75	~75
Platinum	78	195.09	21.45	5.165	4.87	~120
Gold	79	196.97	19.3	4.665	4.93	~80
Lead	82	207.19	11.34	2.704	4.97	~120

Table B.1: Relevant information on possible candidates for scattering targets. The attenuation coefficients and neutron photoproduction cross sections are for 10 MeV γ rays.

Bibliography

[Can01] R. S. Canon. Ph.D. thesis, Duke University, 2001.

[Die88] S. S. Dietrich and B. L. Berman. *Atlas of Photoneutron Cross Sections Obtained with Monoenergetic Photons.* Atomic Data and Nuclear Data Tables 38, March 1988.

[Eva55] R. D. Evans. *The Atomic Nucleus.* McGraw-Hill Book Company, Inc., 1955.

[Iga01] R. Igarashi, 2001. Private Communication.

[Kra92] L. H. Kramer. Ph.D. thesis, Duke University, 1992.

[Lit93] V. N. Litvinenko, J. M. J. Madey, and N. A. Vinokurov. *UV-VUV FEL Program at Duke Storage Ring with OK-4 optical klystron.* In *Proc. of 1993 IEEE Particle Accelerator Conference, Washington D. C.*, page 1442, 1993.

[Lit95] V. N. Litvinenko et al. *Comissioning of the Duke Storage Ring.* In *Proc. Particle Accelerator Conf.*, pages 213–215, 1995.

[Lit96] V. N. Litvinenko and J. M. J. Madey. Nucl. Intr. Meth, **A 375**(1996) 580.

[Mac95] B. E. MacGibbon, G. Garino, M. A. Lucas, A. M. Nathan, G. Feldman, and B. Dolbilkin. Phys. Rev. C, **52**(1995) 2097.

[Mar85] Thomas C. Marshal. *Free-electron Lasers.* Macmillan, Inc., 1985.

[NIS] *http://physics.nist.gov/PhysRefData/contents.html.*

[Par00] S. H. Park. Ph.D. thesis, Duke University, 2000.

[Rin]

[Sab01] A. Sabourov, 2001. Private Communication.

[Sch00] E. C. Schreiber. Ph.D. thesis, Duke University, 2000.

[Vog95] J. M. Vogt, J. C. Bergstrom, R. Igarashi, and K. J. Keeter. Nucl. Intr. Meth., **366**(1995) 100–114.